AD-A172 378 EXPERIMENTAL CONTROL OF SIMULTANEOUSLY EXCITED STRUCTURAL MODES(U) AIR FORCE INST OF TECH WRIGHT-PATTERSON AFB OH SCHOOL OF ENGINEERING 1/1

UNCLASSIFIED R L WRIGHT DEC 85 AFIT/GAE/AA/85D-19 F/G 13/13 NL

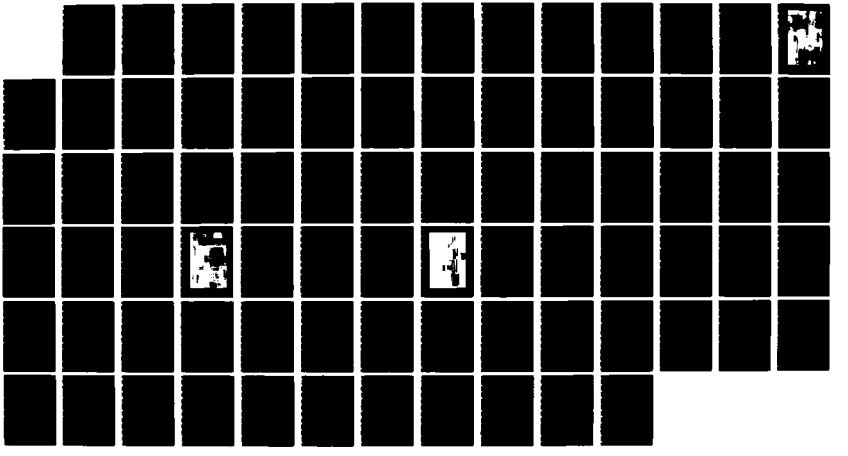

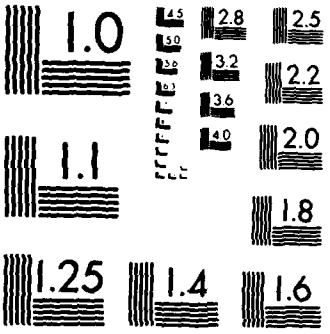

EXPERIMENTAL CONTROL OF SIMULTANEOUSLY EXCITED STRUCTURAL MODES

THESIS

Richard L. Wright Jr.
Captain, USAF

AFIT/GAE/AA/85D-19

DEPARTMENT OF THE AIR FORCE
AIR UNIVERSITY
AIR FORCE INSTITUTE OF TECHNOLOGY

Wright-Patterson Air Force Base, Ohio

EXPERIMENTAL CONTROL OF SIMULTANEOUSLY EXCITED STRUCTURAL MODES

THESIS

Richard L. Wright Jr.
Captain, USAF

AFIT/GAE/AA/85D-19

AFIT/GAE/AA/85D-19

EXPERIMENTAL CONTROL OF SIMULTANEOUSLY EXCITED STRUCTURAL MODES

THESIS

Presented to the Faculty of the School of Engineering

of the Air Force Institute of Technology

Air University

In Partial Fulfillment of the

Requirements for the Degree of

Master of Science in Aeronautical Engineering

Richard L. Wright Jr.

Captain, USAF

December 1985

Preface

The purpose of this experiment was to demonstrate the ability to control structural modes with a lower order controller by a unique modal suppression technique. Some advantages of controllers based on only subsets of a total systems modes include having less complex designs and the possible decentralized control of large structures.

A model of an existing cantilever beam experiment was used in computer simulations of several control designs. Experimental measurements reflected the stability and control predicted by the simulations. However, one-to-one correspondence between simulations and experiments was never realized due to uncertainties in the equipment calibration factors and sensitivity to noise.

Additional studies should be done in this area but preferably on a different model. The new model and equipment should be well defined such that experiment and simulations can be equated. Also, a model with closely spaced modes would provide a good test of the suppression technique and decentralized control.

I would like to acknowledge the help I received from so many individuals in the course of this study. First, Dr. R. Calico, my thesis advisor, for the privilege of working for him on this particular topic, and for his patience in my times of uncertainty. Also, Dr. P. Torvik and Lt Col J. Widhalm for serving as committee members. I am deeply indebted to Maj Hugh C. Briggs for educating me in control theory and helping me for so many hours. Lastly, but certainly not least, I'd like to thank my wife Diane for her help as an engineer, secretary, and mother of our children during these difficult months.

TABLE OF CONTENTS

List of Figures

List of Figures (continued)

List of Tables

Abstract

This experiment demonstrated the application of a lower order controller. A cantilever beam's second mode was controlled without decreasing stability in the remaining modes. This was made possible by eliminating observation spillover.

Computer simulations were conducted to build control designs and to predict their effectiveness. Modal suppression techniques were used on the first and third modes of a cantilever beam while control was applied to mode two; a three mode model. To measure the effect of the suppression technique, an additional control design based on mode 2 alone was also evaluated.

The simulations indicated that the suppressed modes control design would decrease the second mode amplitude without affecting the first or third modes. Simulations also showed that the single mode model would decrease mode 2 responses but also decrease mode 1 stability. These predictions were verified experimentally on the cantilevered beam.

EXPERIMENTAL CONTROL OF SIMULTANEOUSLY EXCITED STRUCTURAL MODES

I. Introduction

Research into the control of vibration modes has heightened with the likely applications toward large, flexible space structures. A particular focus has been on the development of methods which reduce the number of modes necessary to be controlled while maintaining a stable system. This could lead to less complex, lower order controllers capable of decentralized control of several modes. Also, applying these methods to space structures or aircraft could result in reduced requirements for vibration control equipment, and therefore less weight (more payload) and fewer systems to maintain.

The research presented in this report is based on experimental active control of the transverse vibration of a cantilevered beam. The theoretical background was based on previous work by Hungerford (1) and additional modal control principles developed by Coradetti (2). In his research, Hungerford examined the theoretical control of a cantilevered beam by applying methods developed by Balas (3). This method involved the use and placement of sensors and actuators, and a state estimator to compare measured responses with a predefined dynamical model of the structure. While system responses are measured, the estimator would form an estimate of modal participation and a controller would respond by commanding an actuator to eliminate undesired modes. Through computer simulations, Hungerford demonstrated successful control of a cantilever beam's responses.

Hungerford's model included all resonant responses across a frequency band, beginning with the lowest modal frequency. The goal in this experiment however, was to build a lower order controller; one considering only selected modes. By doing so, some uncontrolled modal responses could be driven unstable. This could result from sensor outputs which contain information from uncontrolled modal responses, and control actuator inputs which could excite these same modes. These affects are referred to as observation and control spillover, respectively.

Calico and Janiszewski (4) addressed the causes of spillover and outlined procedures for eliminating it. Classifying modes as controlled, suppressed, and residual, they specifically designed a controller not to excite suppressed modes by eliminating their observability. Having done so, the controller was allowed to affect only a portion of the structure's many modes, while suppressed modes would be used to form a buffer between these and the unmodeled residuals. Given enough bandwidth separation between controlled and residual modes, the system should remain stable. The purpose of this experiment was to account for these classes of modes and to experimentally demonstrate this type of control on a cantilevered beam.

AFIT was invited to conduct this test on an apparatus assembled by the Structural Vibration and Acoustics Branch (FIBG) of the Flight Dynamics Laboratory, Air Force Wright Aeronautical Laboratories (AFWAL), Figure 1. FIBG had already built this testbed for research related to large space structures (LSS) control. As a result, most of the test setup and system identification had already been completed by AFWAL engineers, particularly Major Hugh C. Briggs and Captain Kristin Farry.

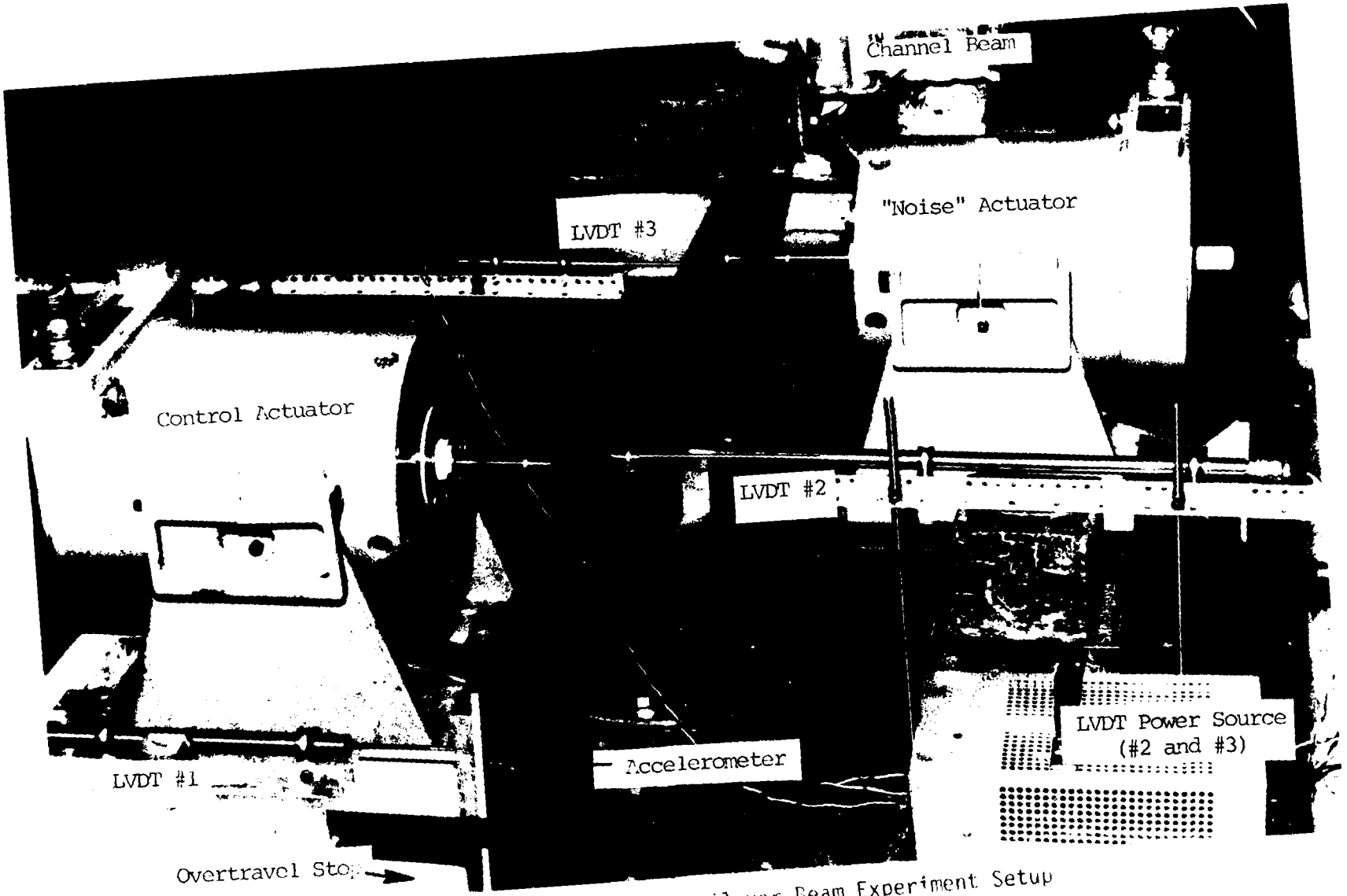

Figure 1. Cantilever Beam Experiment Setup

II. System Identification

The system plant, control, and output matrices were derived by finite element methods (FEM) for an aluminum cantilevered beam, 70in. x 1in. x 4in., with two actuators, Figure 2, Briggs (5). The finite element model consisted of 15 elements with 2 degrees of freedom (DOF) per node: lateral displacement and rotation.

The finite element model was used to assemble the equations of motion for the beam in the following form

$$M\ddot{\bar{q}} + K\bar{q} = D\bar{u} \tag{1}$$

where $\bar{q}$ is a vector of generalized coordinates, M a diagonal mass matrix, K a symmetrical stiffness matrix, D a matrix of actuator coefficients, and $\bar{u}$ an n-vector of inputs, where n equals the number of actuators, Calico (4).

In general, the D matrix consists of n columns, one for each actuator configuration, describing where the force(s) will be applied. Since the actuators will be constrained to being placed at finite element node positions, this matrix is composed of only ones and zeros. The occurrence of a one within D would indicate the presence of an actuator attached at the corresponding node, as determined by the placement within the matrix. A positive one would correlate to a positive force input causing a positive beam deflection; conversely for negative ones. A zero would indicate that there would not be an actuator at the corresponding node.

Now, as a step toward reducing the order of this equation, introduce modal coordinates $\bar{\eta}$ as

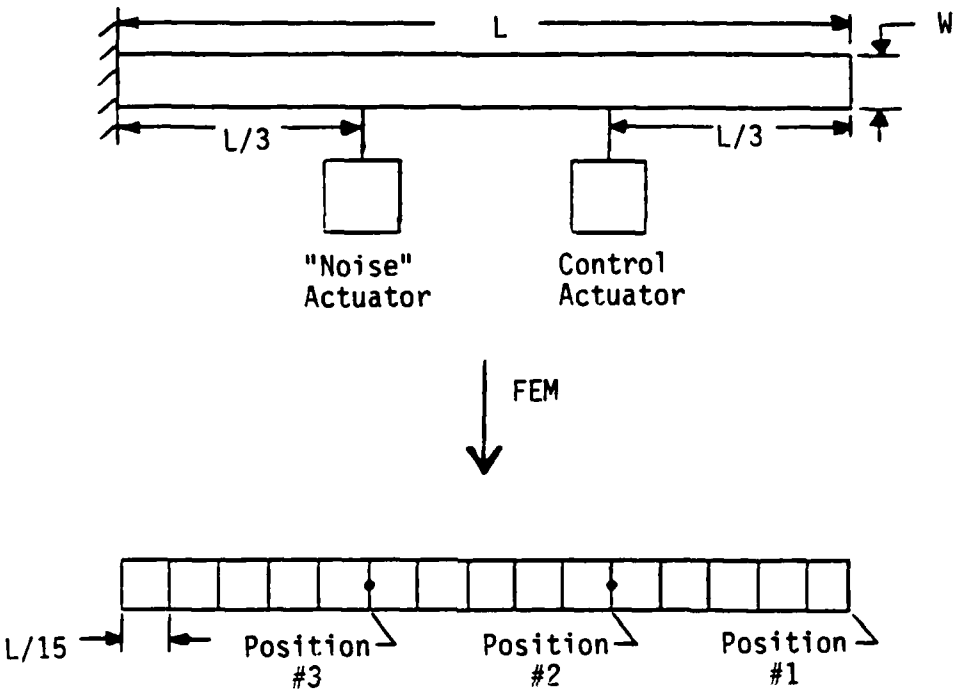

- Point masses added for armature masses

15 elements

L = 70 inches

W = 1 inch

H = 4 inches

E = 10×10^6 psi

Figure 2. Finite Element Model of Cantilevered Beam

$$\bar{q} = \phi\bar{n} \tag{2a}$$

and

$$\dot{\bar{q}} = \phi\dot{\bar{n}} \tag{2b}$$

where ϕ is the modal matrix for the system described by Eq (1). Making substitutions of Eqs (2) into Eq (1) results in

$$M\phi\ddot{\bar{n}} + K\phi\bar{n} = D\bar{u} \tag{3}$$

Multiplying Eq (3) by ϕ^T gives

$$\phi^T M\phi\ddot{\bar{n}} + \phi^T K\phi\bar{n} = \phi^T D\bar{u} \tag{4}$$

Recognizing the following,

$$\phi^T M\phi = [m] \tag{5a}$$

and

$$\phi^T K\phi = [k] \tag{5b}$$

the equations of motion can be uncoupled and Eq (4) rewritten on an elemental level as

$$m_{ii}\ddot{n}_i + k_{ii}n_i = \phi_i^T Du \tag{6}$$

where i represents the element number.

To complete the model, modal damping in the form $c_{ii}\dot{n}_i$ was assumed. While it is realized that this is not the primary damping mechanism in the cantilever beam, it does provide a means to build a linear model which may be used with the linear control techniques of this experiment. The resulting equation of motion may be now be written as

$$m_{ii}\ddot{n}_i + c_{ii}\dot{n}_i + k_{ii}n_i = \phi_i^T Du \tag{7}$$

Dividing by m_{ii}, Eq (7) may be rewritten in the familiar form of

$$\ddot{n}_i + 2\zeta_i\omega_i\dot{n}_i + \omega_i^2 n_i = h_i u \tag{8}$$

where

$$c_{ii}/m_{ii} = 2\zeta_i\omega_i \tag{9a}$$

$$k_{ii}/m_{ii} = \omega_i^2 \tag{9b}$$

and

$$h_i = \phi_i^T D/m_{ii} \tag{9c}$$

Eq (8) now represents a set of independent equations; a diagonal damping matrix $[2\zeta\omega]$, a diagonal matrix of the eigenvalues $[\omega^2]$ (squares of the natural frequencies) and a control vector $\bar{h}$.

For this experiment, the first six modes were modeled. Therefore, from the finite element model only six DOF will be considered and so Eq (8) will be for i = 1, 2,..., 6. Also, only one actuator will be used for control, thus reducing h to a column matrix. To express Eq (8) in first order form and to implement a state space controller, define a state vector x of modal amplitudes (positions and velocities), as

$$x = \begin{Bmatrix} \eta \\ \dot{\eta} \end{Bmatrix} \tag{10}$$

By partitioning x with positions on top and velocities below, Eq (5a) becomes

$$\dot{x} = Ax + Bu \tag{11a}$$

where

$$A = \begin{bmatrix} 0 & I \\ -\omega^2 & -2\zeta\omega \end{bmatrix} \tag{11b}$$

and

$$B = \begin{Bmatrix} 0 \\ h \end{Bmatrix} \tag{11c}$$

where I is a 6x6 identity matrix, $[\omega^2]$ a 6x6 diagonal matrix of the eigenvalues, $[2\zeta\omega]$ a 6x6 diagonal matrix, and B a 12x1 control vector.

Experimental measurements were made on the beam to verify the FEM results. The measured resonant frequencies were found to be lower than those predicted, so modifications were made to the model.

Suspecting possible inaccuracies in the modeling due to the actuator masses, Briggs "tuned" the model by varying each armature mass equally until good agreement with measured data was reached. An increase of 8/5 over the manufacture's published armature mass was established as the "tuned" mass for each actuator.

The resultant FEM resonant frequencies and mode shapes for the reduced model are given in Tables I and II. Each column in Table II represents the beam shape at resonance in increasing order of frequency. Additionally, the first three mode shapes are shown graphically in Figure 3, with sensor positions indicated. Likewise, Figure 4 depicts modes 4, 5, and 6, also with sensor positions indicated, Briggs (5).

TABLE I.
Cantilever Beam Resonant Frequencies

	Resonant Frequency (Hz)					
	Mode 1	Mode 2	Mode 3	Mode 4	Mode 5	Mode 6
Model without Actuators	6.48	40.6	114.0	222.7	-	-
Model with Actuators	6.24	38.1	101.5	220.2	-	-
Tuned model	6.09	36.84	95.9	220.2	343.18	479.06
Measured data	6.06	36.4	96.15	212.53	322.6	454.97

TABLE II.
Finite Element Derived Mode Shapes
for the "Tuned" Model

	Mode Shape					
Position*	Mode 1	Mode 2	Mode 3	Mode 4	Mode 5	Mode 6
1	.4826	.5267	.5363	.4612	-.5125	-.4766
2	.2656	-.1628	-.2938	-.0655	-.1566	-.2323
3	.0809	-.2712	.3272	-.0724	.1505	-.2316

*Reference Figure 2

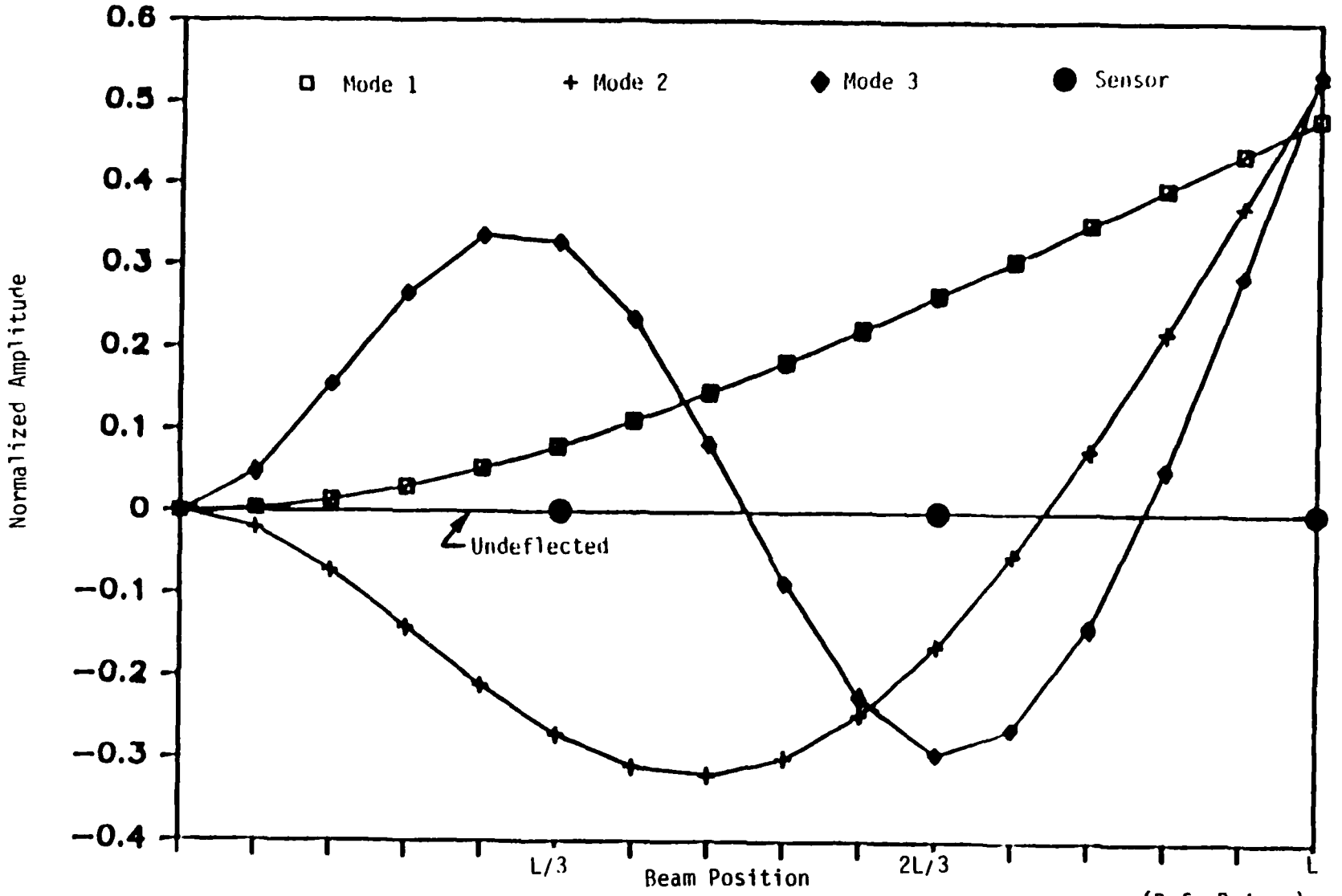

Figure 3. FEM Derived Mode Shapes: Modes 1, 2 and 3 (Ref. Briggs)

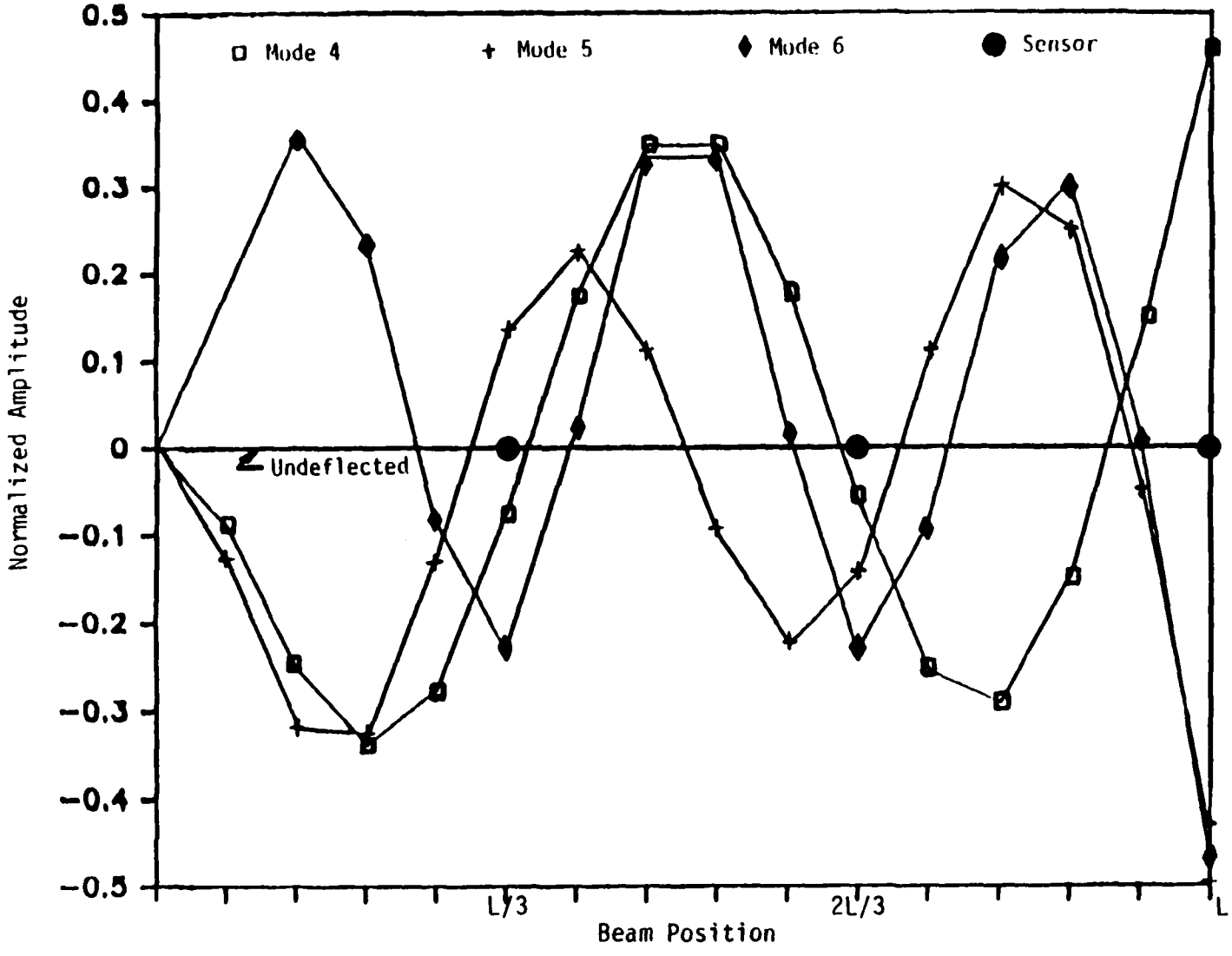

Figure 4. FEM Derived Mode Shapes: Modes 4, 5 and 6 (Ref. Briggs)

Modeling of damping was done by selecting a representative modal value typical for metal structures, $\zeta = 0.01$. Damping was also measured experimentally by first calculating the rate of free decay at resonance, the logarithmic decrement, Thomson (6:29), as:

$$\delta = 1/n \cdot \ln(x_0/x_n) \tag{12}$$

where

x_0 = initial amplitude

and

x_n = amplitude after n cycles

The logarithmic decrement may also be shown to be

$$\delta = 2\pi\zeta/(1-\zeta^2)^{\frac{1}{2}} \tag{13a}$$

which for $\zeta < .1$ may be approximated by

$$\delta \cong 2\pi\zeta \tag{13b}$$

Equating Eqs (12) and (13b), the damping can then be determined from

$$\zeta = (1/(2\pi n)) \cdot \ln(x_0/x_n) \tag{14}$$

Additionally, the finite element model was used to calculate the generalized modal masses. Again, since only the first six modes would be used in the experiment, only those related masses are presented. Generalized masses (m) and damping values are shown in Table III.

Based on the eigenvalues derived from the finite element model results, the plant matrix A from Eq (11b) was formed from Eqs (9a) and (9b). To form the B matrix of Eq (11c), the option to use the actuator at position 2 to input control forces was first established. This, in turn, forms the D vector into a one in the column corresponding to position 2, and 14 zeros in the remaining columns. B is then computed using the m and ϕ values listed in Tables II and III according to Eqs (9c) and (11c).

TABLE III.
Generalized Modal Masses and Damping

MODE	GENERALIZED MODAL MASS	DAMPING ASSUMED	DAMPING MEASURED
1	.00487	.01	.04
2	.00487	.01	.01
3	.00551	.01	nm
4	.00414	.01	nm
5	.00417	.01	nm
6	.00466	.01	nm

nm: not measured

In general, the state space form for feedback to this system would be based on position (p) and velocity (v) sensors, so the output equation would be

$$y = C_p\bar{q} + C_v\dot{\bar{q}} \tag{15}$$

Therefore, in state vector form

$$y = Cx \tag{16}$$

where

$$C = [C_p\phi \,\vdots\, C_v\phi] \tag{17}$$

Only position sensors will be used in this experiment, and they will be located at finite element nodes. Therefore, the C matrix reduces to

$$C = [C_p\phi \,\vdots\, 0] \tag{18}$$

where $C_p\phi$ is an n_{sen} by n matrix, where n_{sen} is the number of sensors used (3) and n is the number of states (6). A listing of this matrix, as well as for A and B, is given in Appendix A.

III. Theory

The objective of this experiment lies in the development of a controller which can ignore some states while controlling others. Since a practical controller would be designed to incorporate only a subset of all possible structural modes, if consideration is not given uncontrolled states a lower order controller could drive them unstable. To build a controller which will account for various modes, classify these modes as controlled (c), suppressed (s), and residual (r), and partition the state vector as:

$$x = \begin{Bmatrix} x_c \\ x_s \\ x_r \end{Bmatrix} \tag{19}$$

Coradetti (2). Suppressed modes will be those considered in the design of the controller specifically not to be excited. These various x vectors may represent any mode or combination of modes, and are not necessarily in any particular order. Similarly, the system state equations may be rewritten using this notation resulting in

$$\dot{x}_c = A_c x_c + B_c u \tag{20a}$$

$$\dot{x}_s = A_s x_s + B_s u \tag{20b}$$

$$\dot{x}_r = A_r x_r + B_r u \tag{20c}$$

and the output as

$$y = C_c x_c + C_s x_s + C_r x_r \tag{21}$$

where the A, B, and C matrices would be composed of the associated controlled, suppressed, or residual modes as indicated.

Based on the controlled state relations, Eq (20a), a controller

force would be given by

$$u = Gx_c \tag{22}$$

where the gain matrix G will be calculated using linear regulator design. Notice that the control term u is included in each of the x state vectors of Eqs (20). As a result, each of these equations, and therefore the system, are coupled by this control force. So by controlling only x_c, it would be possible to inadvertently excite either suppressed or residual modes. This is referred to as controller spillover.

To make use of the control form of Eq (22), the controlled states must first be derived. Since states cannot be measured directly, they must instead be extracted from sensor measurements (i.e. displacement transducers and accelerometers). In practice though, due to system noises and equipment limitations, sensors are not able to provide perfect measurements, therefore an estimator is needed to decipher information provided. This results in estimates of the states, denoted $\hat{x}$. Forming an observer for this system, the state estimates become

$$\dot{\hat{x}}_c = A_c\hat{x}_c + B_cu + K(y - \hat{y}) \tag{23}$$

where the estimated output $\hat{y}$ is

$$\hat{y} = C_c\hat{x}_c \tag{24}$$

The state-estimator gain matrix K will be derived by a Kalman Filter design.

Notice that Eq (23) includes sensor outputs from all states, and as such the controlled model is coupled to these states. This coupling could result in incorrect interpretations of the states, and therefore improper control signals could be generated. This is referred to as observation spillover; where the observation of unmodeled states could

bias state estimates and possibly drive the system unstable.

Methods for eliminating both types of spillover depend on the availability and placement of sensors and actuators. Eliminating either spillover is sufficient for maintaining a stable system, Calico (4). For this experiment, the number and placement of sensors and actuators were dictated by the FIBG supplied setup. Therefore, with three sensors providing observations of the system states, and only one actuator for control, observation spillover was all that could be eliminated.

To eliminate observation spillover, the relations between the gain matrix and the output matrices are constrained as follows:

$$KC_s = 0 \tag{25}$$

$$KC_r = 0 \tag{26}$$

$$KC_c \neq 0 \tag{27}$$

As stated earlier, any practical model will be based on a reduced number of modes. Therefore, assuming a reduced order controller, residual modes will be ignored and only Eqs (25) and (27) will need to be satisfied. Residual modes for this experiment were considered to be modes 4 and above. However, for computer simulation purposes only, modes 4, 5, and 6 were modeled so that controller affects could be monitored in these modes as well.

The solution to Eq (25) can be found through a singular value decomposition (SVD) of the matrix C_s. If C_s is of full rank, a solution exits only when the number of suppressed modes is less than the number of sensors. The SVD results in an orthogonal matrix of left singular vectors (W). By partitioning this matrix into left singular vectors associated with the nonzero singular values (W_r), and left singular vectors associated with the zero singular values (W_q) of C_s, find that

$$W_q^T C_s = 0$$

Letting $T = W_q^T$, the solution to Eq (25) then becomes

$$TC_s = 0 \tag{28}$$

Since the suppressed modes observability has been eliminated, define a new output relation which does not include them as

$$v = Ty \tag{29}$$

Substitution for y from Eq (21) gives

$$v = TC_c x_c + TC_s x_s + TC_r x_r$$

which, ignoring residuals and applying Eq (28), reduces to

$$v = TC_c x_c \tag{30}$$

The design will now be based on

$$\dot{x}_c = A_c x_c + B_c u \tag{31a}$$

$$v = TC_c x_c \tag{31b}$$

$$u = Gx_c \tag{31c}$$

Recalling that the terms of x_c are not directly measurable quantities, introduce state estimates as defined by Eq (23) so that Eqs (31) become

$$\dot{\hat{x}}_c = A_c \hat{x}_c + B_c u + K^*(v-\hat{v}) \tag{32}$$

$$\hat{v} = TC_c \hat{x}_c \tag{33}$$

and

$$u = G\hat{x}_c \tag{34}$$

where

$$K^* T = K$$

The state-estimate equation then becomes

$$\dot{\hat{x}}_c = (A_c + B_c G - KTC_c)\hat{x}_c + KTy \tag{35}$$

IV. Solutions to System Equations

Solutions to the system equations were determined by using a VAX 11/785 computer equipped with $MATRIX_x^{TM}$ software Ref (7). $MATRIX_x^{TM}$ is a powerful program, providing simple means for interactively solving complex matrix operations; eigenvalue solutions, matrix inversion, and singular value decomposition routines, to name but a few. It also provided for control design and linear dynamic analysis either in continuous-time or discrete-time. Plots of results, system frequency responses for instance, were also easily generated.

For this experiment, $MATRIX_x^{TM}$ was used to solve for system eigenvalues, estimator gains (K), control gains (G), singular value decomposition of suppressed state matrices, system frequency responses, system eigenvalues, and formulation of matrices to be used within the experiment control equipment (array processor).

To initiate computations, A, B, and C matrices were defined for controlled (mode 2), suppressed (modes 1 and 3) and three residual modes (modes 4, 5 and 6), see Eqs (20). Next, the open-loop response of the reduced order system was determined by solving for the eigenvalues of

$$A_{ol} = A_c - KTC_c \tag{36a}$$

where

$$A_{ol} = \text{open-loop system matrix} \tag{36b}$$

$$K = \text{optimal state-estimator gain matrix} \tag{36c}$$

and T derived from

$$TC_s = 0 \tag{36d}$$

Solving for the transformation matrix (T) was done such that Eq (36d) was satisfied. Solving for K was then based on a Kalman filter optimum

state-estimator design for the A_c and TC_c matrices, and noise covariance matrices formed from plant disturbance noises and measurement noises. In this process, the following cost functional was minimized to establish K.

$$J = \int_0^\infty (x^T Q_{xx} x + y^T Q_{yy} y)\, dt \tag{37}$$

The plant noises were set equal to

$$Q_{xx} = \begin{bmatrix} 1 & 0 \\ 0 & 1 \end{bmatrix} \tag{38a}$$

and the measurement noise to

$$Q_{yy} = \overline{Q}_{yy} [\ I\ ] \tag{38b}$$

where $\overline{Q}_{yy}$ is a constant.

Perturbations of the noise values were done until the open-loop eigenvalues of mode 2 resulted in damping values of $\zeta = .01$. That is, while holding A_c and TC_c fixed, the magnitude of $\overline{Q}_{yy}$ was varied until the estimated damping nearly equaled the assumed damping.

A frequency response curve was plotted at each $\overline{Q}_{yy}$-value and the damping determined using the half-power points method, Thomson (6:72-73).

$$\zeta = \frac{\omega_2 - \omega_1}{2\omega_n} \tag{39a}$$

where

$$\omega_{1,2} = \text{sideband frequencies at .707 x resonant amplitude} \tag{39b}$$

and

$$\omega_n = \text{resonant frequency} \tag{39c}$$

Figures 5 thru 7 show the results of this process for various $\overline{Q}_{yy}$ values. The response in Figure 7, at $\overline{Q}_{yy} = 10$, represented a system with $\zeta = .01$, and so it was used to establish the state-estimator gain K.

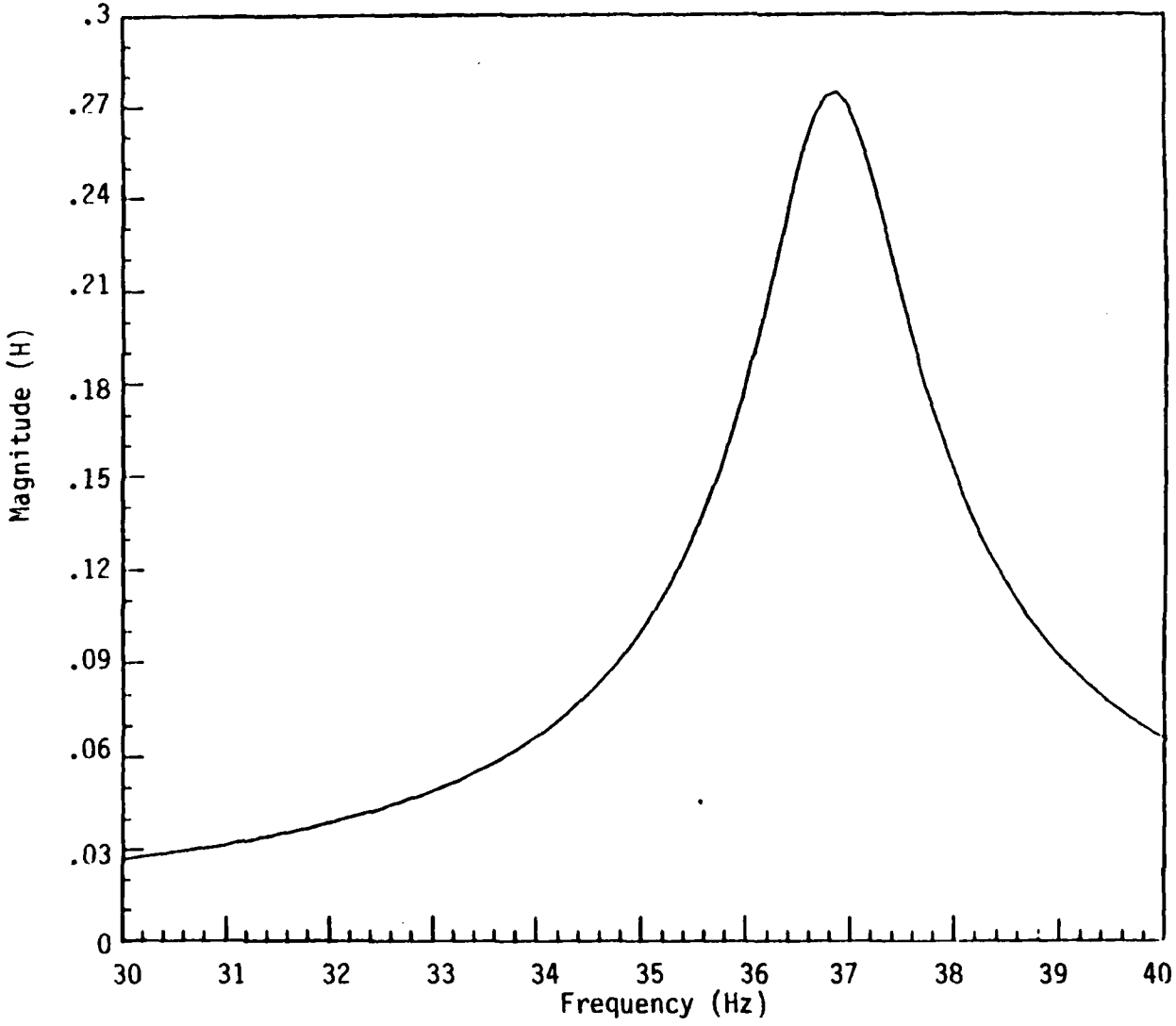

Figure 5. Frequency Response Curve for $\overline{Q}_{yy}$ = .1

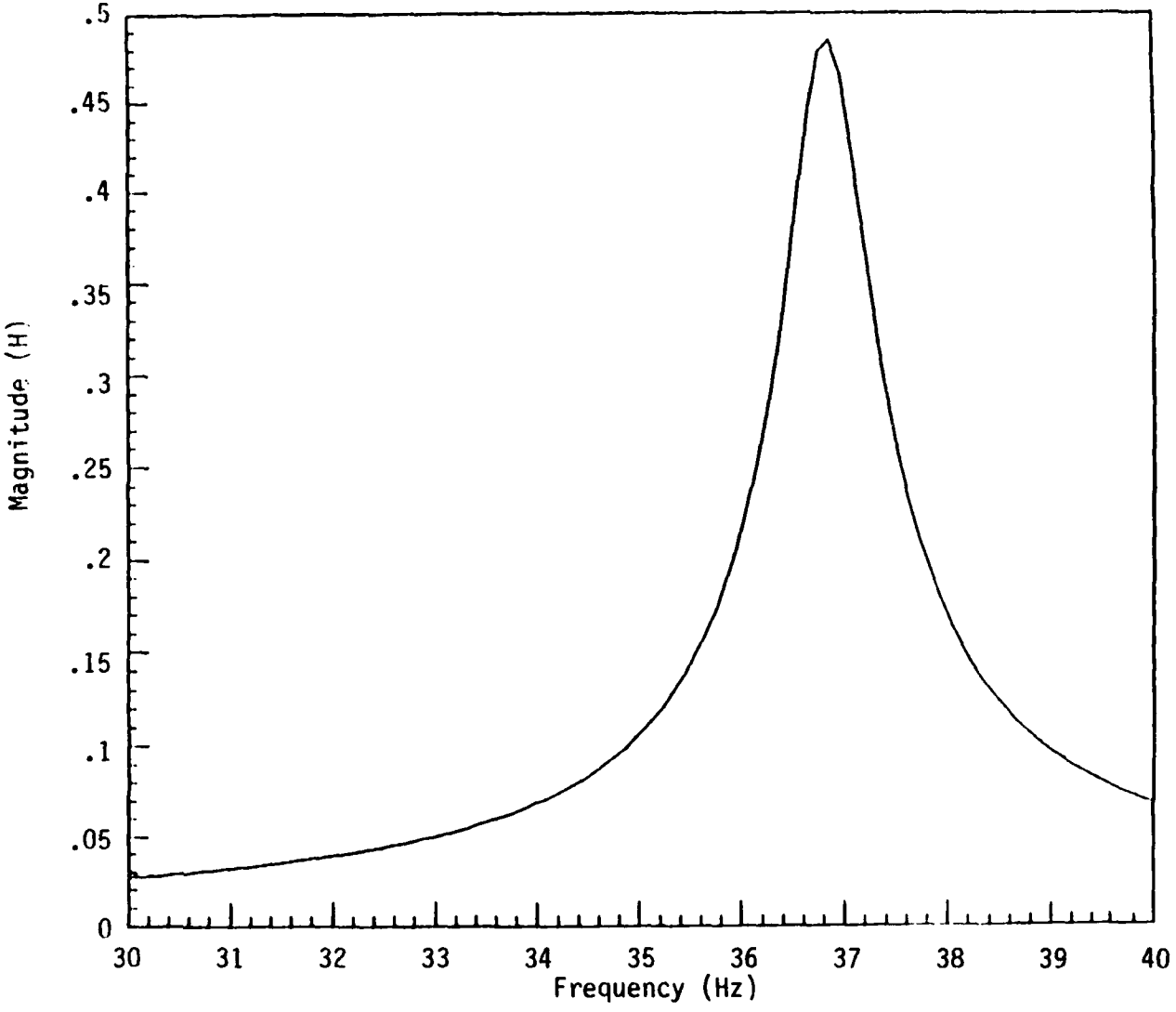

Figure 6. Frequency Response Curve for $\overline{Q}_{yy} = 1.0$

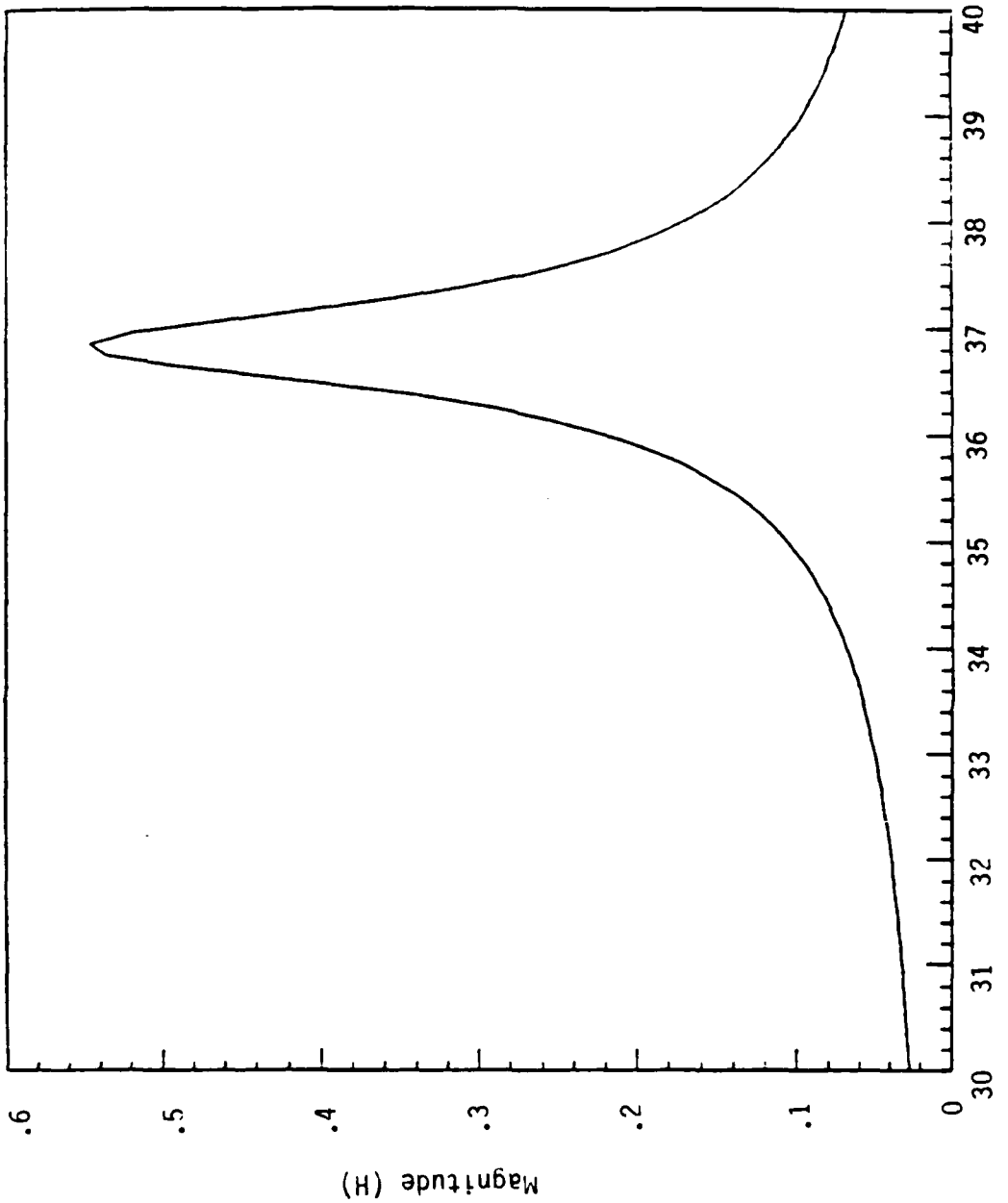

Figure 7. Frequency Response Curve for $\bar{Q}_{yy}$ = 10.0

With the gain matrix K determined, the control gain G was then calculated. This was done by linear regulator design using the plant matrix A_c, control vector B_c, and design weighting matrices on states (R_{xx}) and forces (R_{uu}). Similar to the estimator design, the following cost functional was minimized for the controller design

$$\text{Cost} = \int_0^\infty (x^T R_{xx} x + u^T R_{uu} u)\, dt \tag{40}$$

The weight matrices were chosen as

$$R_{xx} = \begin{bmatrix} 1 & 0 \\ 0 & 1 \end{bmatrix} \tag{41a}$$

and

$$R_{uu} = \bar{R}_{uu} [\, I \,] \tag{41b}$$

where $\bar{R}_{uu}$ is a constant. By decreasing the magnitude of $\bar{R}_{uu}$, an increase of control authority results.

As with the estimator design, the regulator gains were calculated at various values of the weight penalty R_{uu} while holding A_c, B_c, and R_{xx} fixed. At each R_{uu}, the closed-loop system eigenvalues were calculated for the six mode model. Eigenvalue movement in the controlled mode, mode 2, indicated increased damping (larger negative real parts); while little, if any, movement was detected in the remaining modes.

Figure 8a shows the movement of the eigenvalues where $\bar{R}_{uu}$ was increased from .01 to .1 by .01 increments. Damping was calculated from these plots by

$$\zeta = -\text{Re}(z)/|z| \tag{42}$$

where z is the eigenvector.

Damping in mode 2 decreased as the penalty was increased. The scale in Figure 8a was too small to detect movement on mode 1, so that portion

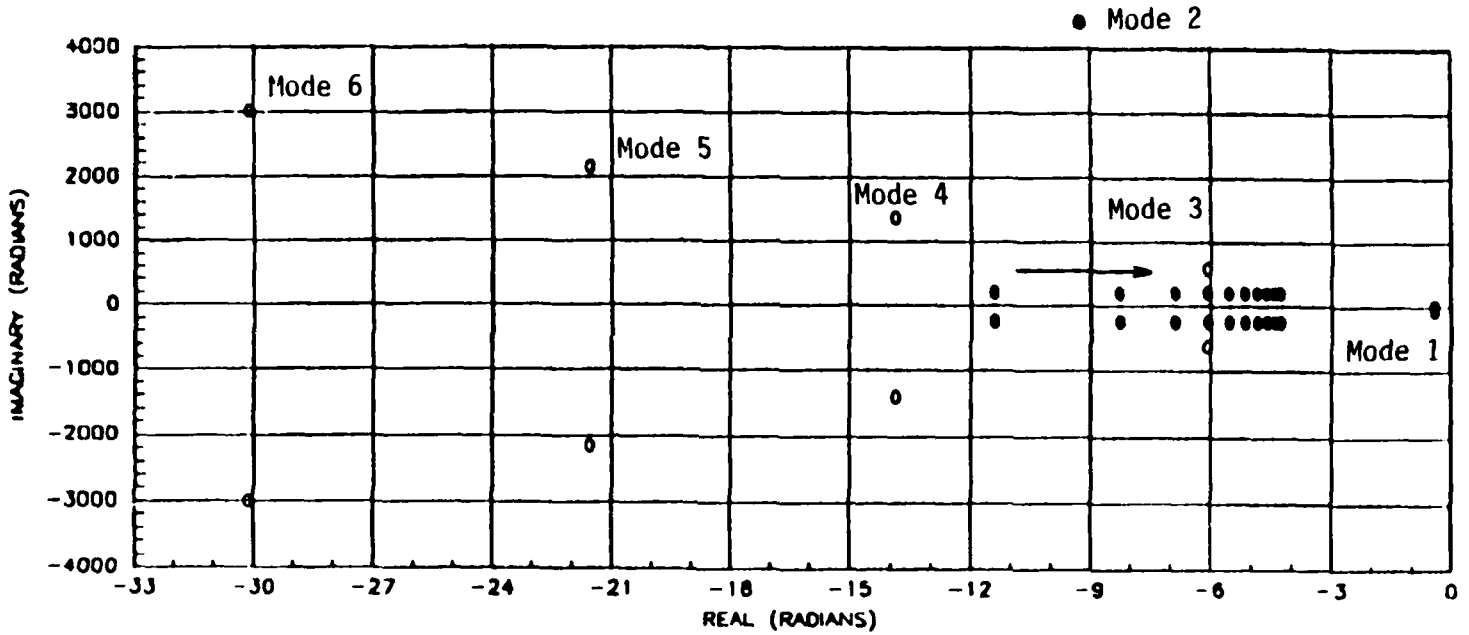

Figure 8a. Closed-loop Eigenvalues for R_{uu} = .01 to .1, Suppressed Model

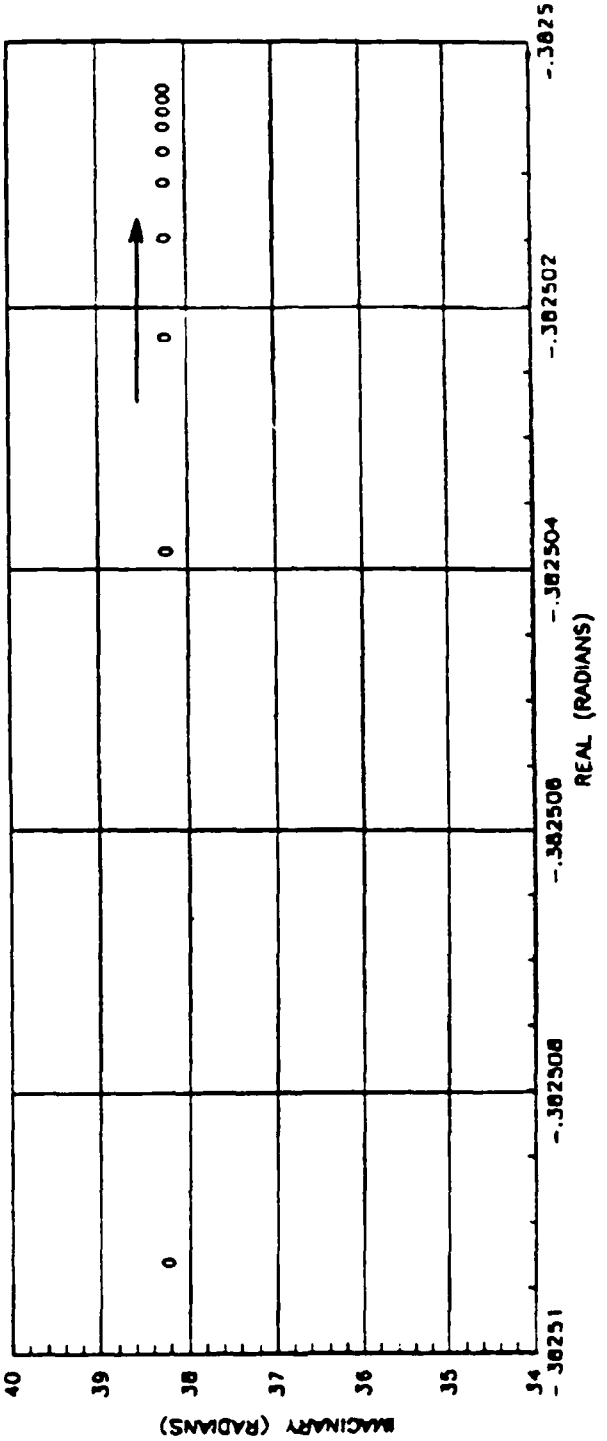

Figure 8b. Expanded View on Mode 1 Eigenvalues

was replotted in Figure 8b. The scale had to be expanded such an extreme amount ($\Delta\omega$ = .00001 rads) that any movement perceived, although in a more stable direction, was beyond the numerical accuracy of this analysis.

Now, having several control designs, the continuous-time system equations were required to be discretized for use in the control equipment. To do so, the following relationships were used from Eqs (34) and (36)

$$\dot{\hat{x}}_c = (A_c - B_c G - KTC_c)\hat{x}_c + KTy \tag{43}$$

and

$$u = G\hat{x}_c \tag{44}$$

where Eq (43) may be abbreviated for closed-loop (cl) form as

$$\dot{\hat{x}}_c = A_{cl}\hat{x}_c + KTy \tag{45}$$

Discretizing Eqs (44) and (45) into time steps k, based on a sampling rate f, Ref (8:102), results in

$$\hat{x}_{k+1} = \exp(A_{cl}dt)\hat{x}_k + [\exp(A_{cl}dt) - I]\, A_{cl}^{-1}\, KTy_k \tag{46}$$

and

$$u_{k+1} = G\hat{x}_k$$

where dt=1/f.

The form used by the array processor was, Ref (9)

$$\begin{Bmatrix} u_{k+1} \\ \hat{x}_{k+1} \end{Bmatrix} = \left[\begin{array}{c|c} F_{11} & F_{12} \\ \hline F_{21} & F_{22} \end{array}\right] \begin{Bmatrix} y_k \\ \hat{x}_k \end{Bmatrix} \tag{47}$$

where for this experiment, but not in general,

$$F_{11} = 0 \tag{48a}$$

$$F_{12} = G \tag{48b}$$

$$F_{21} = [\exp(A_{cl}dt) - I]\, A_{cl}^{-1} KT \tag{48c}$$

and

$$F_{22} = \exp(A_{c1}dt) \tag{48d}$$

These matrices were produced by Matrix$_x$™ for several design parameters.

An alternate design based solely on mode 2, without suppression of modes 1 and 3, was created for a comparison to the suppression model. Similar system equations were satisfied except that a SVD was not required and so the observation vector remained as

$$\hat{y} = C_c\hat{x}_c$$

Therefore this design was based on the following state-estimate relation

$$\dot{\hat{x}}_c = (A_c - B_cG - KC_c)\hat{x}_c + Ky \tag{49}$$

with the control force defined by

$$u = G\hat{x}_c \tag{50}$$

Simulations of this control design were done using Matrix$_x$™, resulting in a predicted decreased stability in the first mode. This is indicated in plots of the eigenvalues for increased controller authority which show mode 1 damping to decrease as the second mode's increases, Figures 9a and 9b. As before, the scale was expanded to show mode 1 movement. While this scale is an order of magnitude larger than that in Figure 8b, it too is to small to make quantitative predictions on mode 1 stability. These designs were also discretized for use on the PC-1000.

In summary of the simulations, the suppressed modes model indicated mode 2 controllability without decreasing stability in any others. The single mode model without suppression however, indicated mode 1 instability with increased control on mode 2.

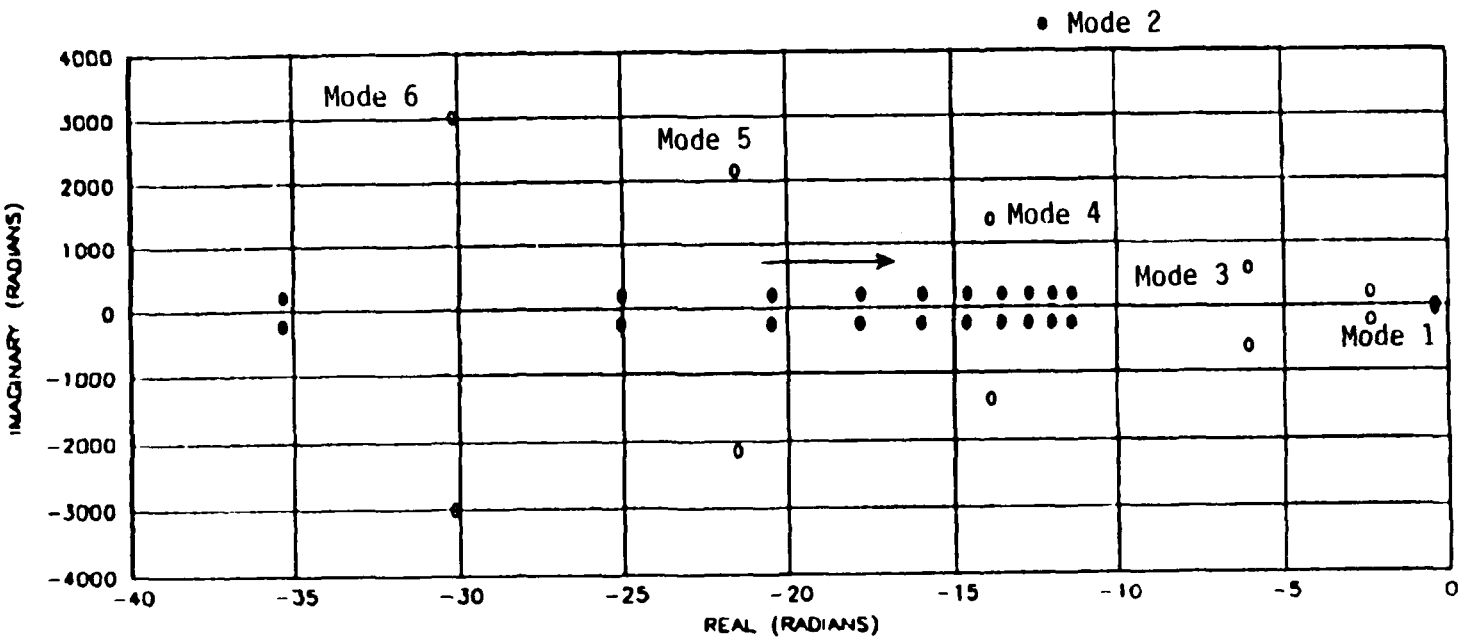

Figure 9a. Closed-loop Eigenvalues for R_{uu} = .001 to .01, Single Mode Model

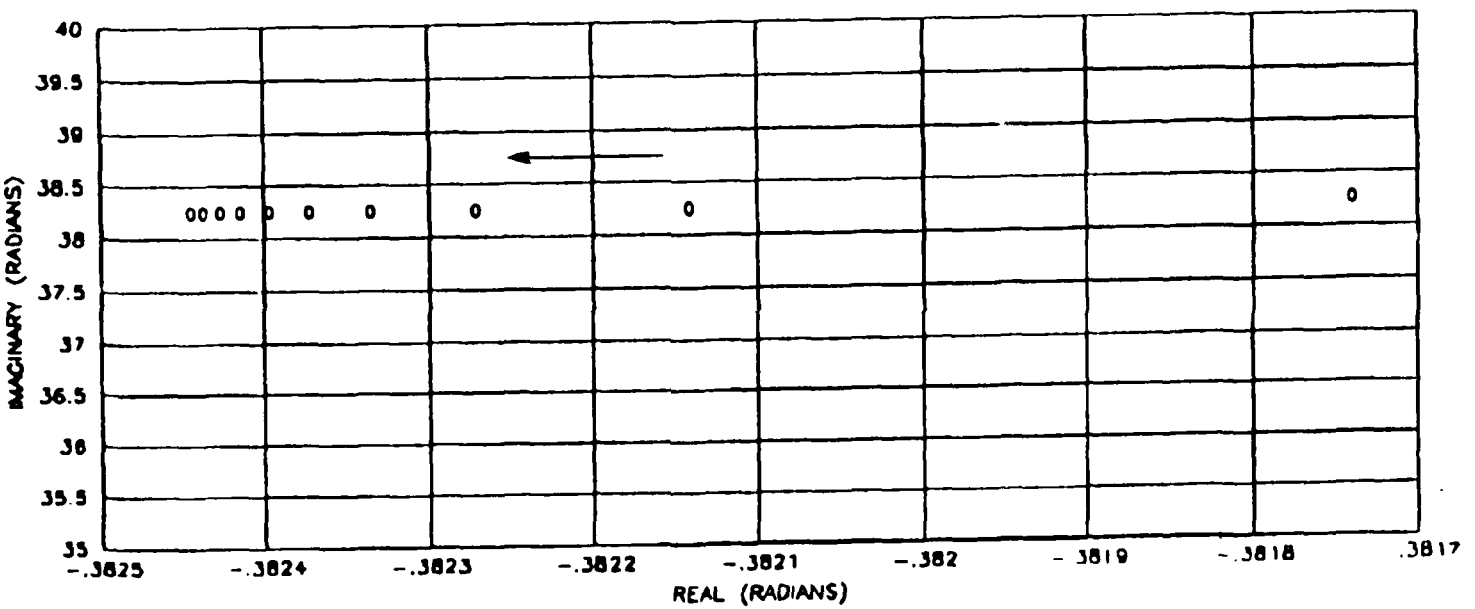

Figure 9b. Expanded View on Mode 1 Eigenvalues

V. Experimental Apparatus

The cantilevered beam experiment was located in Building 461, Area B, Wright-Patterson AFB, Ohio, Figure 1. This setup was built by the Fight Dynamics Laboratory (FDL) as part of their research efforts in the control of large space structures (LSS). There were tests being done concurrently by FDL engineers so modifications to the setup were limited. The only change made to accommodate this test was to add position sensors at beam positions 2 and 3. A list of the equipment used is given below in Table IV and a wire diagram of the setup is shown in Figure 10.

Beam Characteristics

The cantilevered beam's physical characteristics are listed on Figure 2 and is depicted in Figure 1. It was made from an aluminum beam 78 inches long, 4 inches high, and 1 inch wide; 8 inches of which made up the clamped end. The beam was mounted on a steel table which also supported the actuators and sensors. An I-beam was used to provide enough height for the beam to be conveniently connected to the actuators. The I-beam was reinforced with end plates and webs which were welded in place. Two channel beams were attached to the top of the I-beam, each with two bolts, and the beam fastened between these by four bolts. Lead weights and sandbags were laid on this mount assembly to reduce structural ringing experienced in initial tests.

Sensors and Actuators

Estimation of modal states was based on measurements made by three position sensors, linear variable differential transformers (LVDTs). The tip LVDT (position 1) was on hand from earlier experiments while the remaining two were added for this experiment. The LVDTs are made of thin

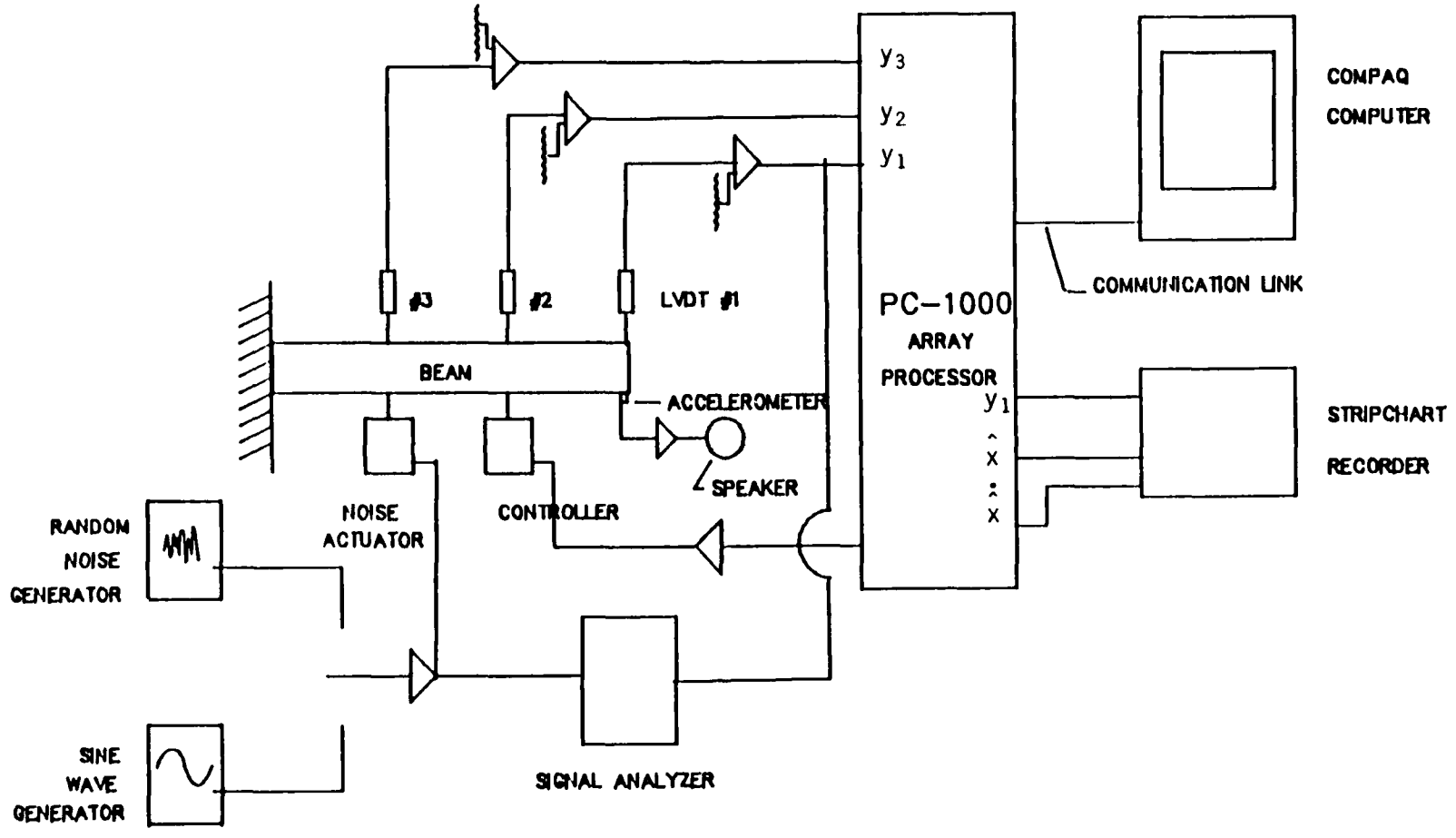

Figure 10. Wire Diagram of Experiment Setup

TABLE IV
Experimentation Equipment List

Item	Manufacture, Model
Actuators and Power Supply	Unholtz-Dickie, Model 4
Sinusoidal Signal Generator	Wavetek, Model IIIB
Random Noise Generator	Hewlett Packard, Model 3722A
LVDT: #1	Schlumberger, Model 583
#2	Schaevitz, Type 3000 HC-D
#3	Schaevitz, Type 1000 HC-D
Power Supply (± 15Vac) for LVDT #1	FIBG In-house Assembled
Power Supply (± 15Vdc) for LVDT #2 and #3	Systron Donner Corp, Trygon Model TL8-3
Accelerometer	Vibrametrics, M1000A
Oscilloscope	Tektronix, 5A14N 4 channel Amplifier and 5B12N Dual Time Base
Digital Voltmeter	Fluke, 8050A Digital Multimeter
Analog Signal Processor	Comdyna, Model 808
Cross-channel Spectrum Analyzer	Wavetek, Rockland Model 5820A
Stripchart Recorder	Watanabe Instruments Corp., Linearcorder, Mark VI, WR3101
Experimentation Host Computer	Compaq Portable Computer
Array Processor	Systolic Systems Inc, PC-1000
Line Printer	IBM, Model 5152002
Plotter	Hewlett Packard, Model 7470A
Electric Glue Gun	Bostik, Thermogrip Electric Glue Gun
Mainframe Computer	Digital Electronics Equipment, VAX 11/785
Video Camera	RCA Newvicom Color Video Camera, Model CC015 with TGP1500 Video Recorder and TV

rods (1/8 to 3/16 inch diameter) which are free to slide inside long tubes. The internal diameters of these tubes were only slightly greater than the rods. The depth of these rods within the tubes determined the voltage output of these devices and therefore the position (displacement) of the beam at that sensor location. Each rod was attached to the beam with glue from an electric glue gun. The frequency range for each LVDT was from 0 to over 500 Hz.

The tip LVDT, LVDT #1, had a ±2 inch stroke capability, an output sensitivity of 2 volts/inch, and was operated by a ±15Vac power supply. Maximum displacements expected at this position were ±1.5 in. It was clamped to a small channel beam which was anchored to a concrete block and the steel table. This LVDT was being used by FIBG in their tests on the beam and as such was not subject to being modified.

The LVDT at position 2, LVDT #2, had a ±3 inch stroke capability and an output sensitivity of 3.5 volts/inch. It was clamped to a small angle iron which was anchored to lead weights and the steel table. Maximum displacements expected here were ±.9 in. This LVDT was operated from a ±15Vdc power supply which also powered the remaining LVDT at position 3 (LVDT #3).

LVDT #3 was mounted in the same manor as LVDT #2, but it's stroke capability was only ±1 inch with a sensitivity of 10.2 volts/inch. The maximum displacements expected here were ±.3 in.

In addition to LVDTs, an accelerometer was mounted to the beam tip. Its output was sent to a speaker to provided the experimenter audible feedback of the beam's response. This was particularly useful since the beam was in a chamber separate from the testing equipment in the "Control Room". FIBG also supplied a camera and TV monitor so that the test could

be observed from this room as well.

The beam excitation and control forces were provided by two electrodynamic actuators, each capable of generating 75 pounds force and having an approximate sensitivity of 15 lbs/volt. They were firmly clamped to the table to eliminate potential sliding or rotations. One actuator was placed at position 2 as the controller and the other at position 3 as the "noise" source. A wood block was placed on the concrete block at the beam tip to provide a safety stop in case the actuator displacements became too large.

Due to the uncertainty in the actuator sensitivity, the exact force levels generated during tests were unknown. However, estimates of these levels based on 15 lbs/volt would indicate a 10 lb maximum from the controlling actuator and 15 lbs from the "noise" actuator. Attempts to measure this sensitivity were made but the dial which is used to adjust it was inadvertently turned at the end of the experimental test runs. This eliminated the ability to determine the actuator sensitivities used during these experiments.

The actuators were attached to the beam by 4in. long x 5/16in. diameter threaded rods. One end of each rod was screwed into the armatures and the other into threaded holes in the beam. Two nuts were on each rod; one was tightened against the armature and the other against the beam to keep the rods from backing out during tests. These rods were tapered to 1/8in. diameter along a 1.5in. center section. This was done to create a relatively weak link so the rods would break in bending before damage to the actuators would occur through excessive side loads. This is standard practice in vibrations tests to protect expensive actuator equipment from unexpectly high forces.

Internal compensation loops within each actuator allowed them to operate independently. Therefore, when one actuator caused a deflection of the beam at the other actuators location, that actuator would not resist the deflection with a repulsive force. The control console for this equipment is shown in Figure 11.

Signal Processor

An analog signal processor was used for the outputs of the LVDTs and inputs to the actuators, Figure 11. The LVDTs were wired through potentiometers within the processor so that the bias (dc offset) could be removed from the outputs.

The concurrent FDL tests had the actuator command signals channeled through the signal processor as well. The AFIT experiment however, used random and sinusoidal generators to control the voltage to the noise actuator, while the controller (within an array processor) adjusted the voltage to the other actuator. Therefore, the signal processor was set to unity gain on these signals, although sign changes occurred.

The sign changes on the actuator signals also occurred on the LVDTs. This was the result of sending signals through the particular amplifiers within the processor which invert the signal. The end result was that a positive signal from the controller to the actuator at position 2 caused the output from the analog processor to be positive on LVDT #1 and #2, but negative on LVDT #3. This sign change was compensated for within the C matrix, described in the Solutions section, by changing the sign on the third row elements which describe LVDT #3 positions.

Signal Generators

Random noise and sinusoidal signal generators, were used as the source of beam excitation for the actuator at position 3. The frequency

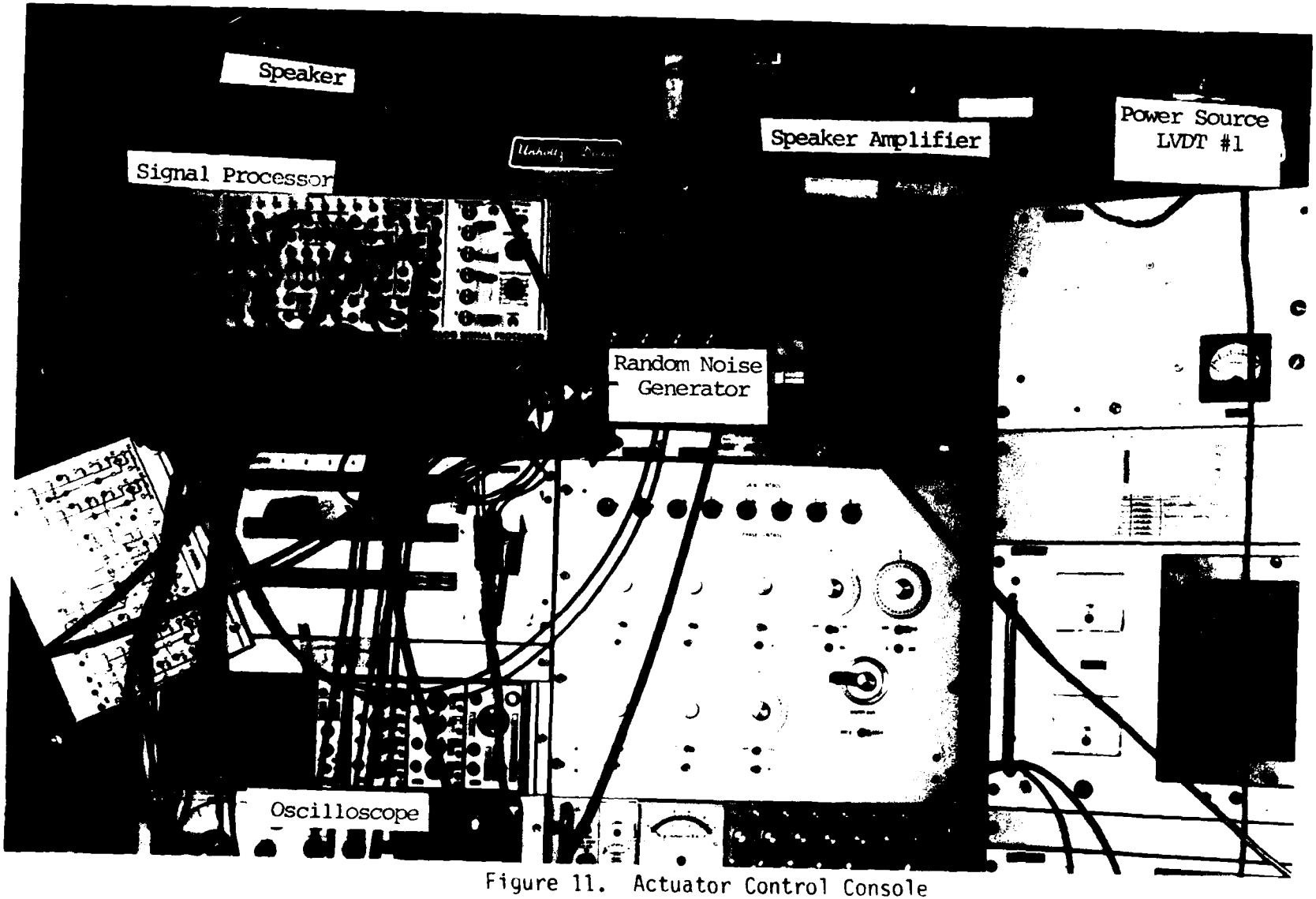

Figure 11. Actuator Control Console

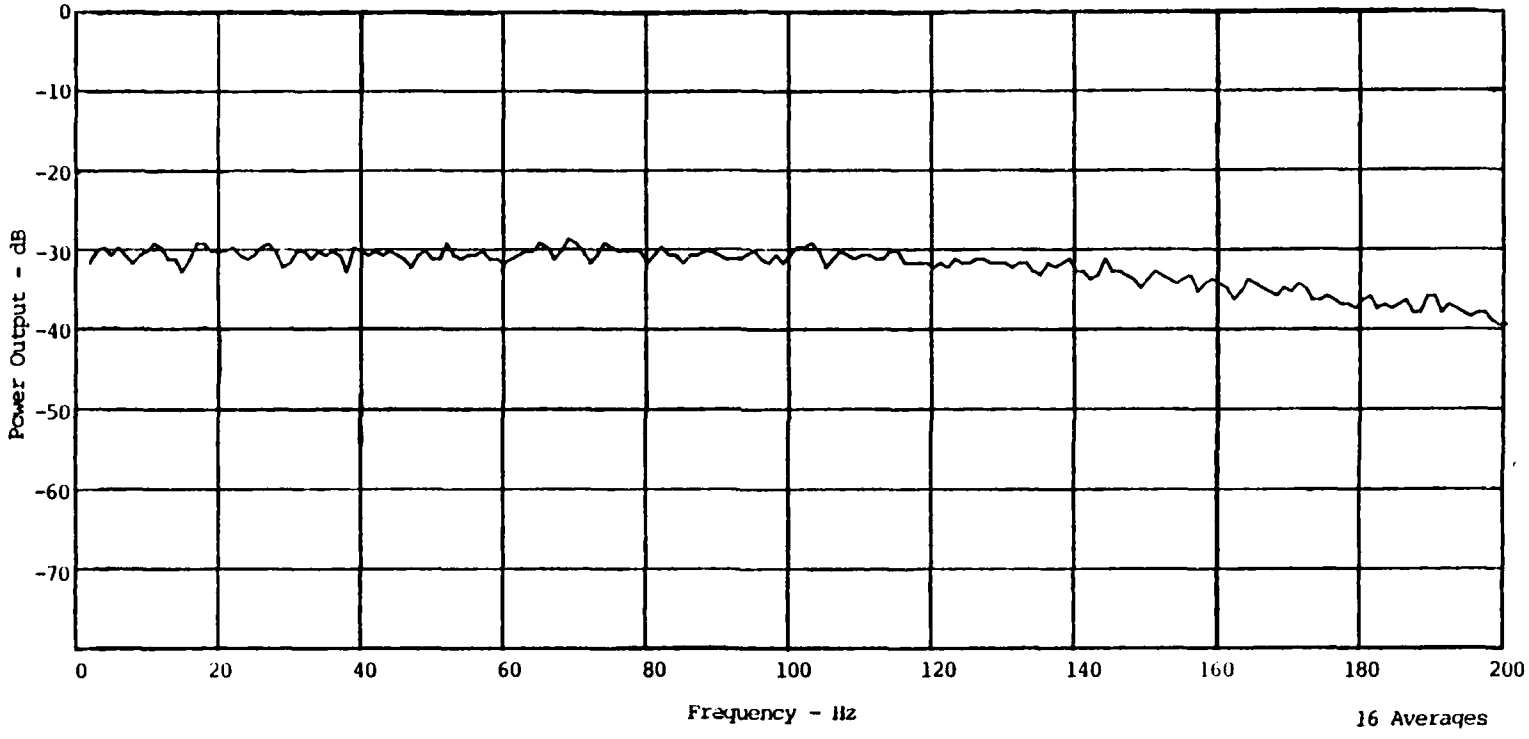

Figure 12. Random Generator Frequency Content, 0 to 150 Hz

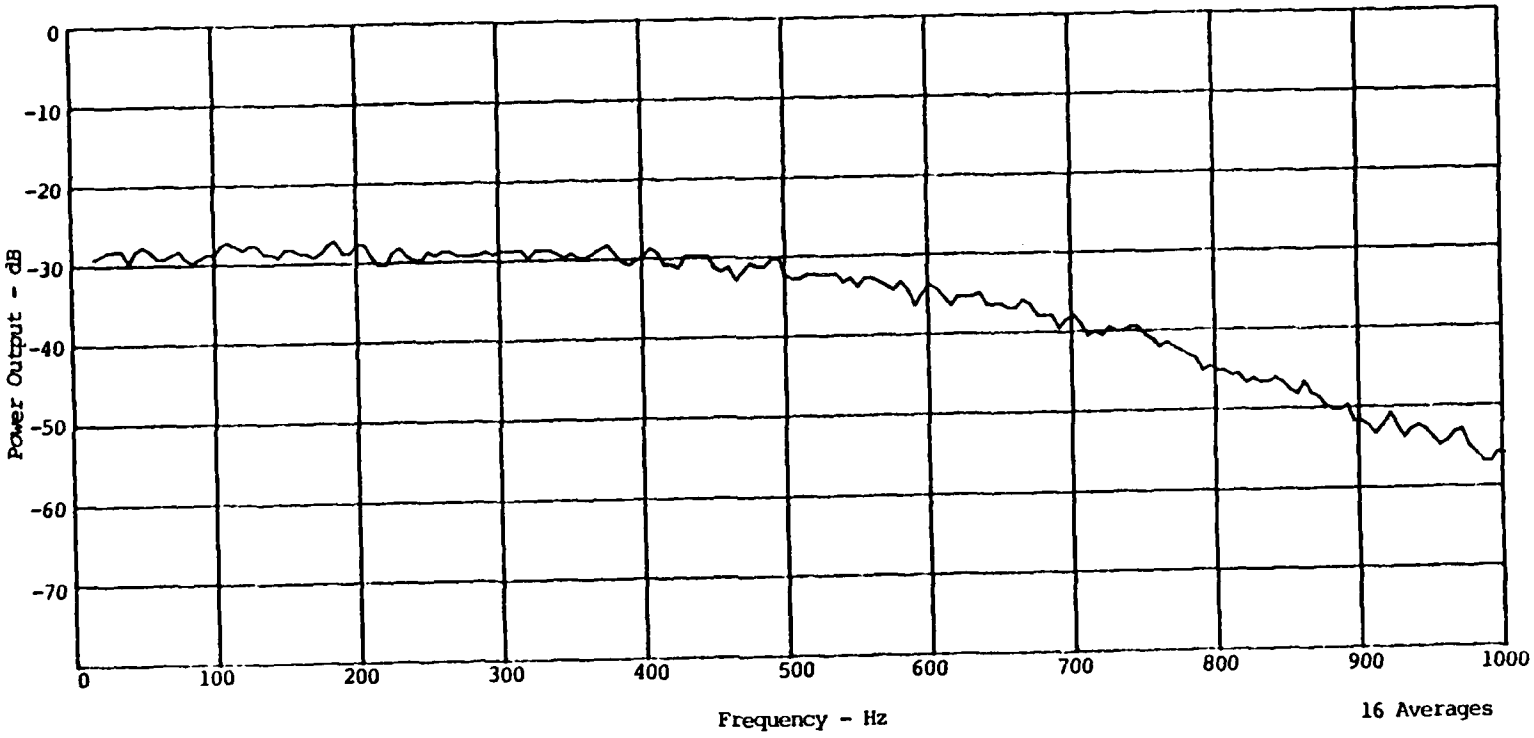

Figure 13. Random Generator Frequency Content, 0 to 500 Hz

range of the random signal generator was adjustable from zero to several peak frequencies; 150 and 500 Hz maximums were used. A frequency content plot is given for each of these ranges in Figures 12 and 13; these show the signal rolloff to be sufficiently beyond the 100 and 500 Hz ranges which were tested. The sinusoidal generator was tunable over a 1 to 100 kHz frequency range and it's output voltage was adjustable from 0 to 1.73 volts.

Array Processor and Host Computer

An array processor was used to acquire the LVDT data and to send control force information to the actuator at position 2. The array processor used was a PC-1000 Systolic Array Processor, Ref (9), Figure 14. This was a desktop, high speed parallel processor designed by Systolic Systems Inc. for real-time data acquisition, and estimation and control applications. The PC-1000 has 16 analog input/output channels with 12 bit resolution; internal computations are done in 32 bit, floating point arithmetic (6 decimal accuracy). It provides programmable sample rates (Hz), signal range (volts), and input gain and output attenuation for each channel.

A host computer is required to operate the PC-1000; it must be IBM Personal Computer compatible and operate under MS-DOS. The software program from Systolic Systems, LABWARE, permits the user to set data acquisition parameters, create data acquisition and engineering design (F matricies) files, edit files, list files to a printer (sample printout in Appendix A), compile engineering files into machine executable code for the PC-1000, and to transmit this data to the PC-1000. The host computer used was a Compaq Portable Computer.

The LVDT output signals (from the analog processor) were input to

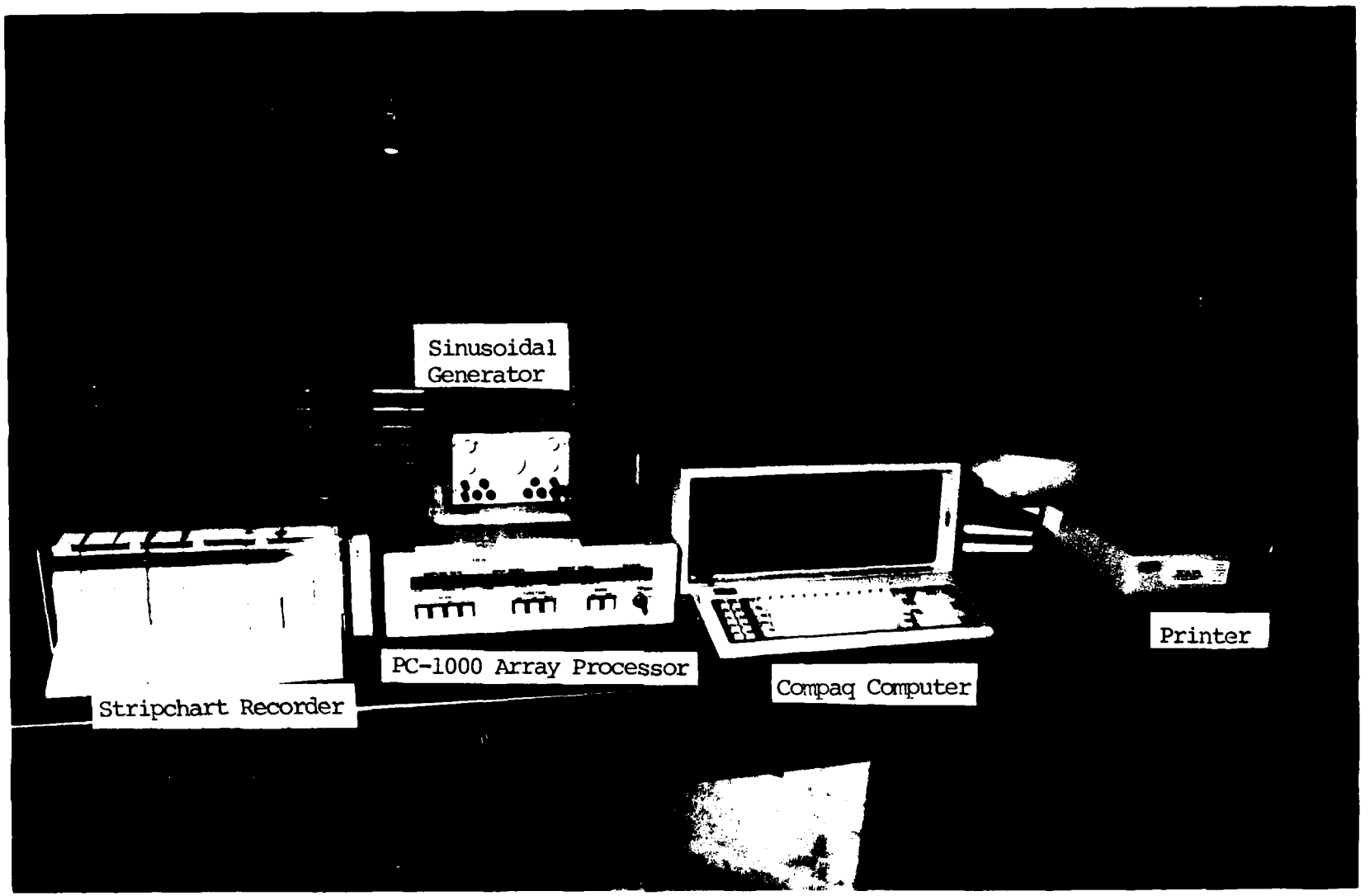

Figure 14. Host Computer and Array Processor

the PC-1000 backpanel. LVDT #1, #2, and #3 were input to channels 1, 3, and 4 respectively (channel 2 was inoperative). The control actuator signal was output on channel 3. State estimates, $\hat{x}_k$ and $\dot{\hat{x}}_k$, were output on the stripchart recorder on channels 11 and 12. LVDT #1 output was also recored on the stripchart, but without going through the array processor hardware.

Spectrum Analyzer

A spectrum analyzer, a Wavetek model, was used to produce the plots from the experiment. These plots include transfer function magnitude versus frequency for LVDT #1 output and the signal from the analog processor to the "noise" actuator. The Wavetek vertical axis is scaled in decibels (dB), with the 0 dB reference at 1 volt, and the horizonal axis is linear in frequency. Screen dumps of its display were able to be made through a connection to a Hewlett Packard plotter. This was the source of the frequency response curves made during the experimental portion of this test.

VI. Experimental Procedure

Initial tests measured the resonant frequencies and damping. To do so, the equipment was activated and allowed to warm up for 15 minutes. The actuator at position 2 was then excited by output from the sinusoidal generator. The frequency was increased from 1 Hz until the accelerometer output voltage peaked, as determined by monitoring its output on an oscilloscope. Peak voltages established the resonant frequencies; those found were as listed in Table I.

To measure damping, LVDT #1 output was recorded on the stripchart during free decay from resonance. This was done by exciting the beam with the sinusoidal signal generator at a resonant frequency, a sine dwell test. While the stripchart recorded LVDT #1 output, the wire carrying the excitation signal was disconnected. This process was repeated four times at modes 1 and 2 to insure repeatability and accuracy. Figure 15 shows the LVDT output for two of these tests.

Next, with simulations completed on $MATRIX_X^{TM}$, control designs were loaded into the PC-1000 array processor. To do so, the Compaq computer was first loaded with the Systolic LABWARE program which is used to create and transfer the design file from disk storage to the PC-1000.

LABWARE was first used to define data acquisition parameters. For this experiment these were: 1000 Hz sample rate, ±5 volt operating range, and unity input and output gains. This information was then compiled by the LABWARE program into machine executable code for use by the PC-1000.

Next, the discretized system model was input, see Appendix A for a sample of this input. These files were also compiled for PC-1000 use. As many as eight models could be stored in the Compaq at one time,

Mode 1, 6 Hz, Free Decay

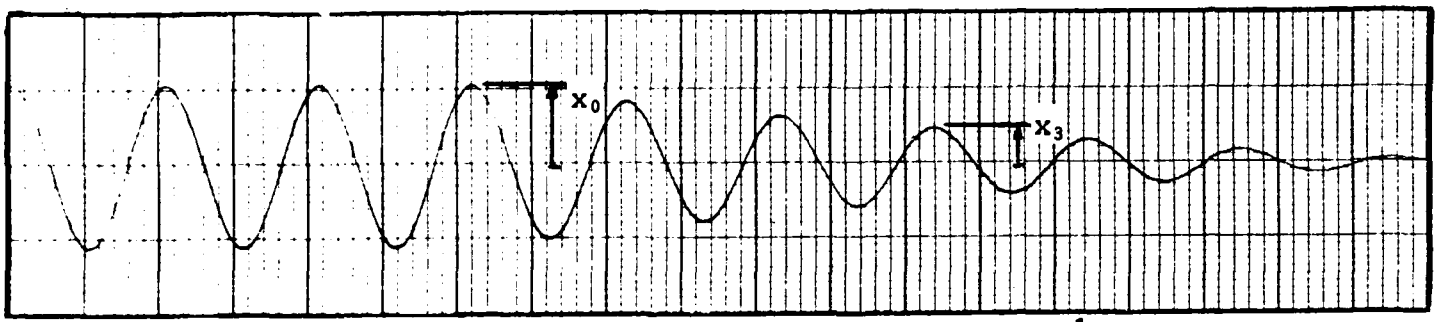

$$\zeta_1 \cong \frac{1}{3*(2\pi)} \ln(11/5) = 0.042$$

Mode 2, 36 Hz, Free Decay

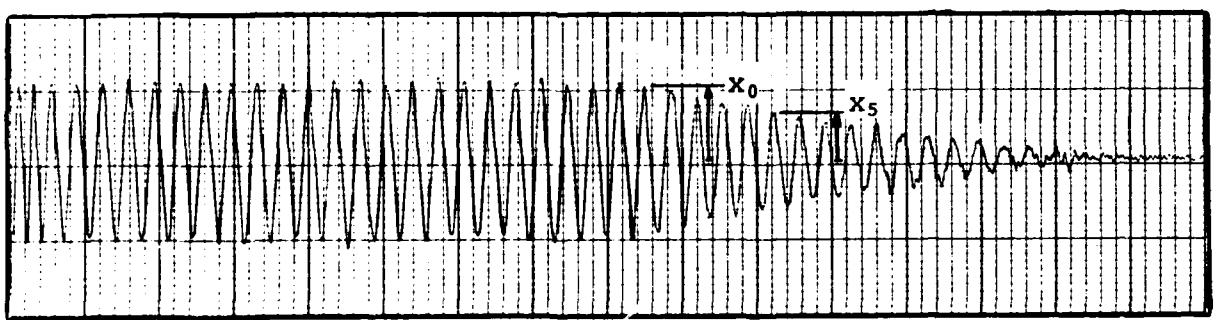

$$\zeta_2 \cong \frac{1}{5*(2\pi)} \ln(10/6.5) = 0.013$$

Figure 15. Stripchart Damping Measurements

allowing for changes to alternate designs in real-time. This capability was used to gradually increase the amount of controller authority while monitoring the system stability.

Having prepared control designs on the array processor, the actuator and sensor equipment was activated. After the warm up period, each LVDT output bias was eliminated. This was done by monitoring individual LVDT outputs on a digital voltmeter while adjusting related potentiometers on the analog computer. Adjustments were made until the bias was less than 1 mV. Both actuators were on at this time, but neither were given force signal inputs.

The first test to be run using the PC-1000 was to test the stability of an estimator model. To do this, a sine wave generator was used to drive the beam. The PC-1000 was then put into the "RUN" mode and the frequency was manually swept from 1 to 200 Hz while the output of the estimator was recorded on the stripchart. The output voltage on the sine wave generator was varied according to the frequency; less voltage was needed at the higher frequencies. The frequency would be held at each of the first three resonances to see if the estimator recognized them. In the case of the suppressed mode model, no state estimate responses were expected at the first and third modal frequencies. However, at the second mode, position and velocity state estimate responses were expected to show on the stripchart as sine waves. An open-loop power spectrum plot was made from the output of LVDT #1 to form the basis of the control design effectiveness at mode 2 resonant conditions.

Following open-loop measurements, a control design was loaded into the PC-1000. The first design would attempt to increase the modal damping by only a small amount. The beam would again be driven through a

frequency range to test the controller's response and system stability. Gradually, control authority was increased while the output from LVDT #1 was used in forming power spectrum plots of the system response.

Following sine dwell testing, random excitation was used to excite the beam. The frequency range and power output were varied for several stages of testing. The range was varied from 0.1 V to 0.3 V over 0 to 150 Hz, and later to 500 Hz. Initially, as with sinusoidal testing, only an estimator was used in the design while open-loop transfer function magnitude plots were generated for each condition. Gradually, increases to authority gain were tested and transfer function magnitude plots generated.

The alternate control design, mode 2 control without suppression on modes 1 and 3, was tested in the same manor. Close attention had to be paid to this phase of tests since it was predicted by simulations to be an unstable design. This proved to be true, so input force levels during sine dwell and random excitation had to be lower than those for the suppressed mode model, depending on the amount of control authority in the design. The wooden stop also played an important role during these tests in limiting unstable beam displacements.

VII. Results and Discussion

The results of the control designs were determined by plotting the tip position LVDT output for open and closed-loop responses. From these, changes in tip displacement amplitude in the first three modes are easily seen. Damping calculations were made however, by measuring logarithmic decrements from free decay tests. Damping was not calculated from these plots because of windowing effects of the signal analyzer on such low damping (ζ<.05).

Modal Suppression Model

Results from tests of the control design controlling mode 2, and suppressing modes 1 and 3, to random excitation are given in Figures 16 through 18; successive figures are for increased control authority. These figures are plots of the transfer function magnitude of LVDT #1 to the "noise" signal sent to the actuator at position 3. Figure 16 shows only a slight decrease in mode two amplitude at R_{uu} = .1 compared to the open-loop response. Decreasing the weight penalty to R_{uu} = .01 resulted in more reduction, Figure 17. Finally, Figure 18, at R_{uu} = .001, shows substantial reduction in mode two, a 9 dB decrease. Notice there are no discernible changes in modes one and three. Tests were also done for 1 to 500 Hz excitation to examine changes in the fourth thru sixth modes. Figure 19 shows the result of this excitation for R_{uu} = .01.

Sine dwell tests, where the beam was harmonically excited in the second mode, were also done on these same designs, Figures 20 through 22. Figure 20 is again for R_{uu} = .1, and indicates an amplitude reduction of 9 dB compared to the open-loop response. Figure 21, R_{uu} = .01, shows a reduction of 15 dB, and Figure 22, R_{uu} = .001, shows a 17 dB drop. These

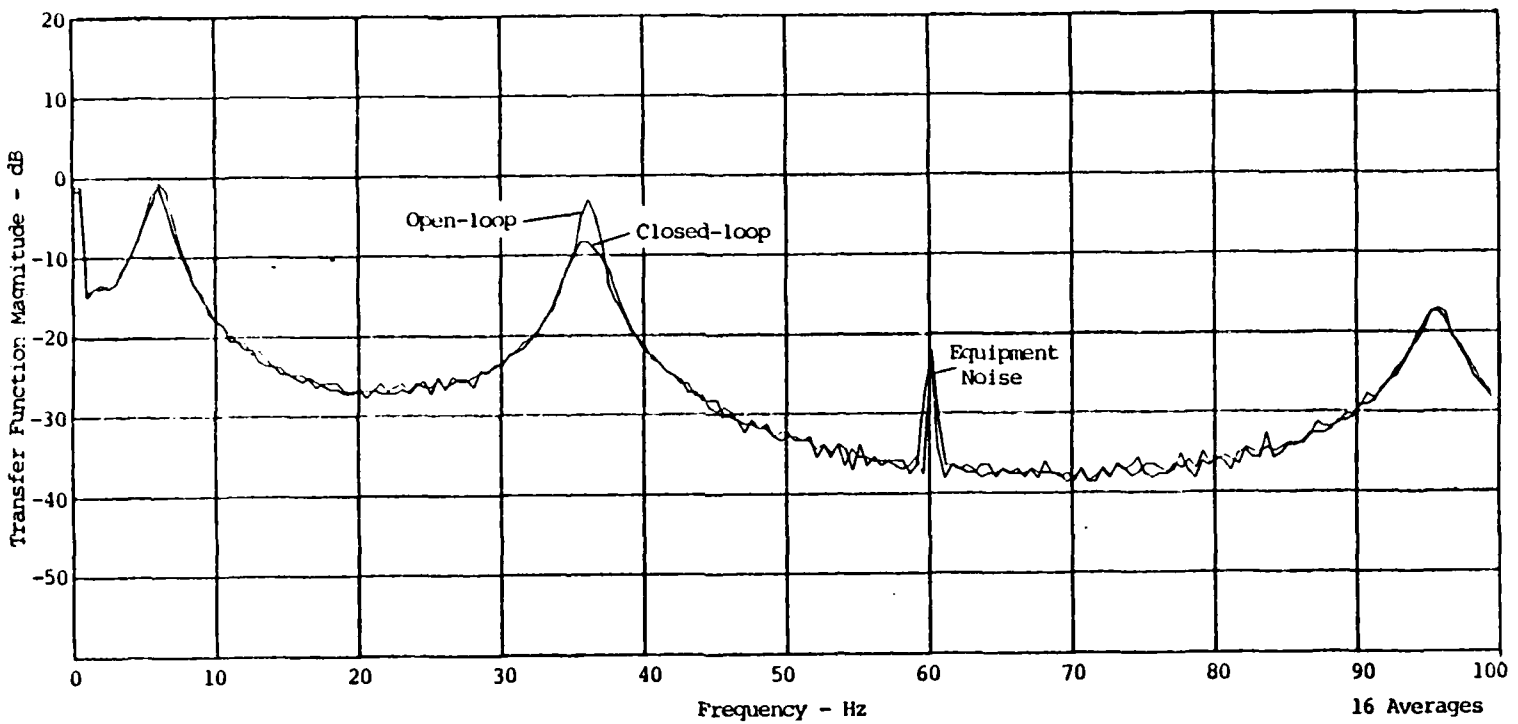

Figure 16. Suppressed Mode Model, R_{uu} = .1, Random Excitation

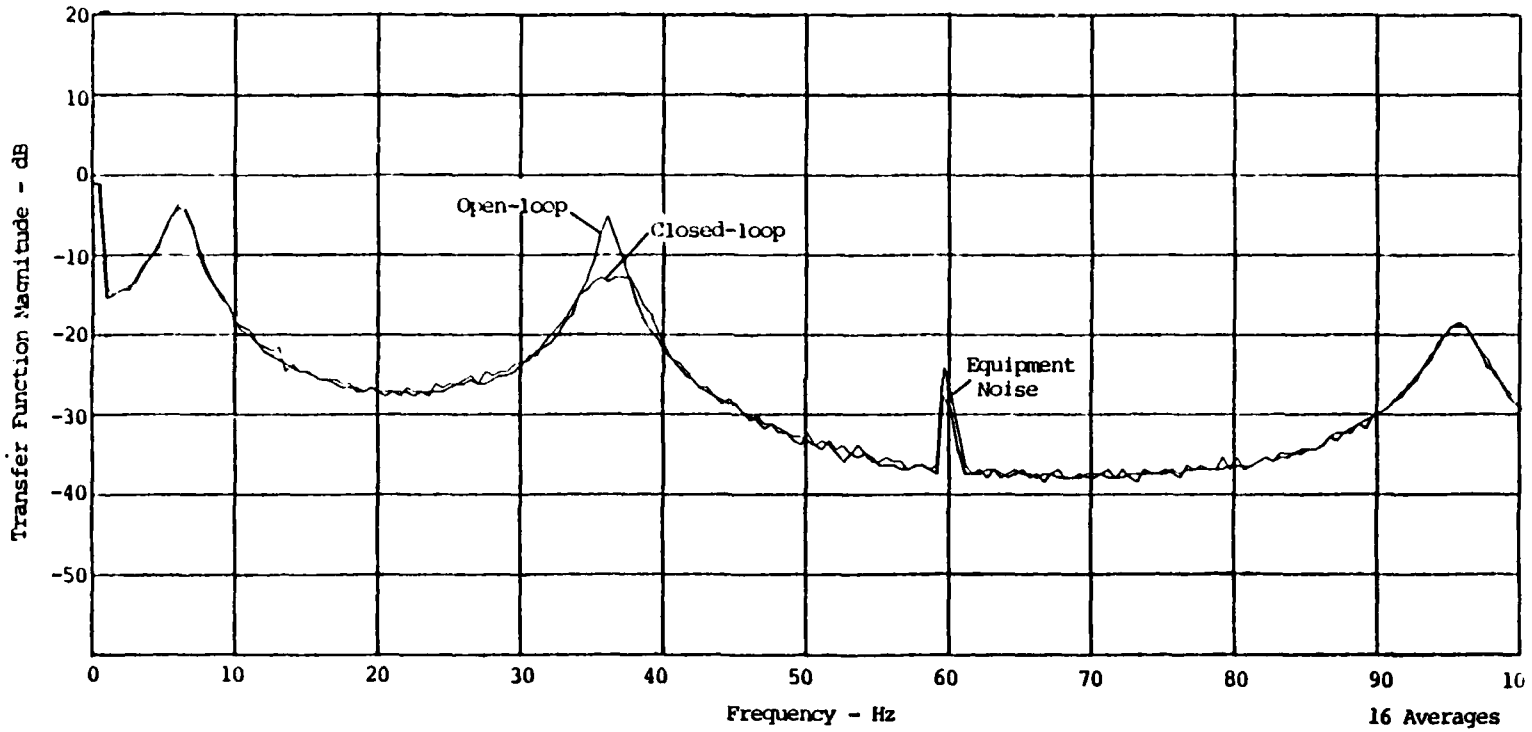

Figure 17. Suppressed Mode Model, R_{uu} = .01, Random Excitation

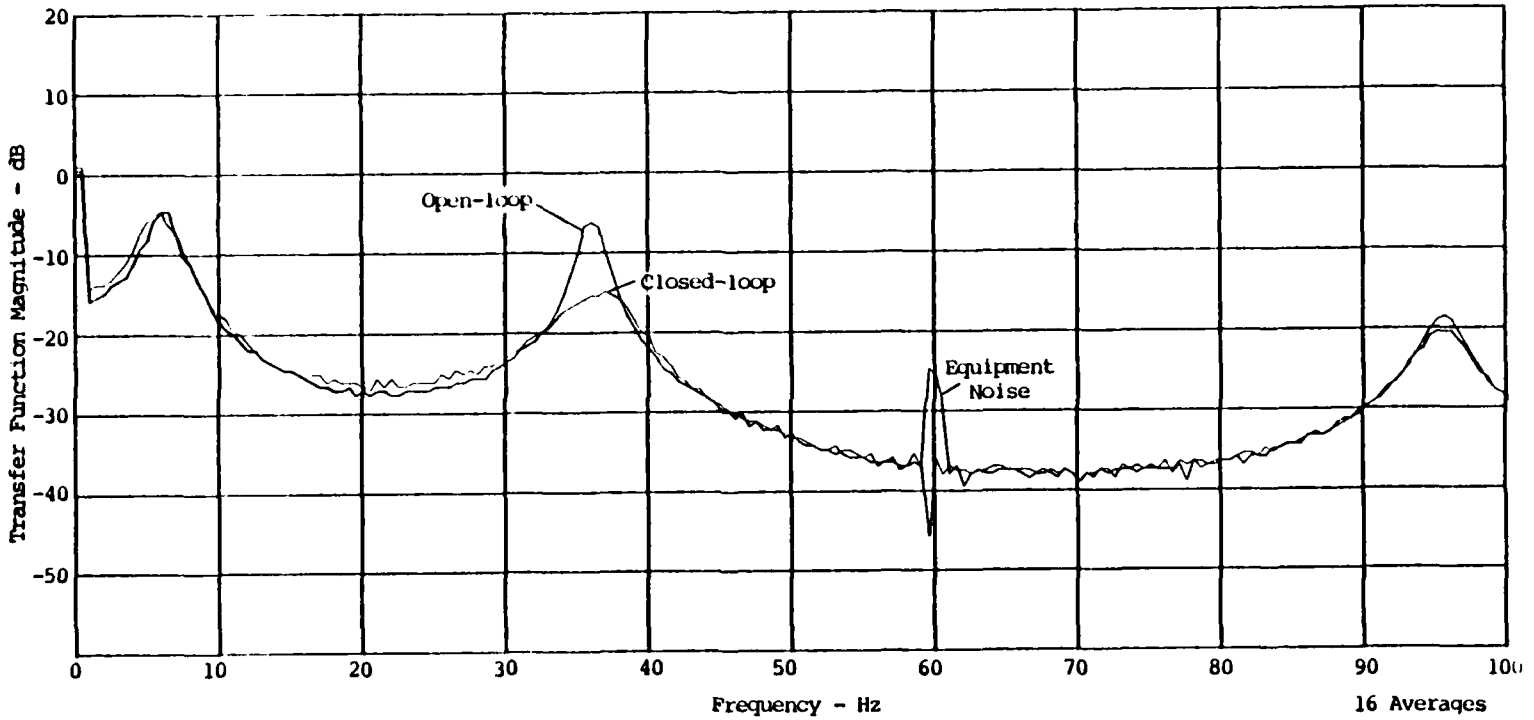

Figure 18. Suppressed Mode Model, R_{uu} = .001, Random Excitation

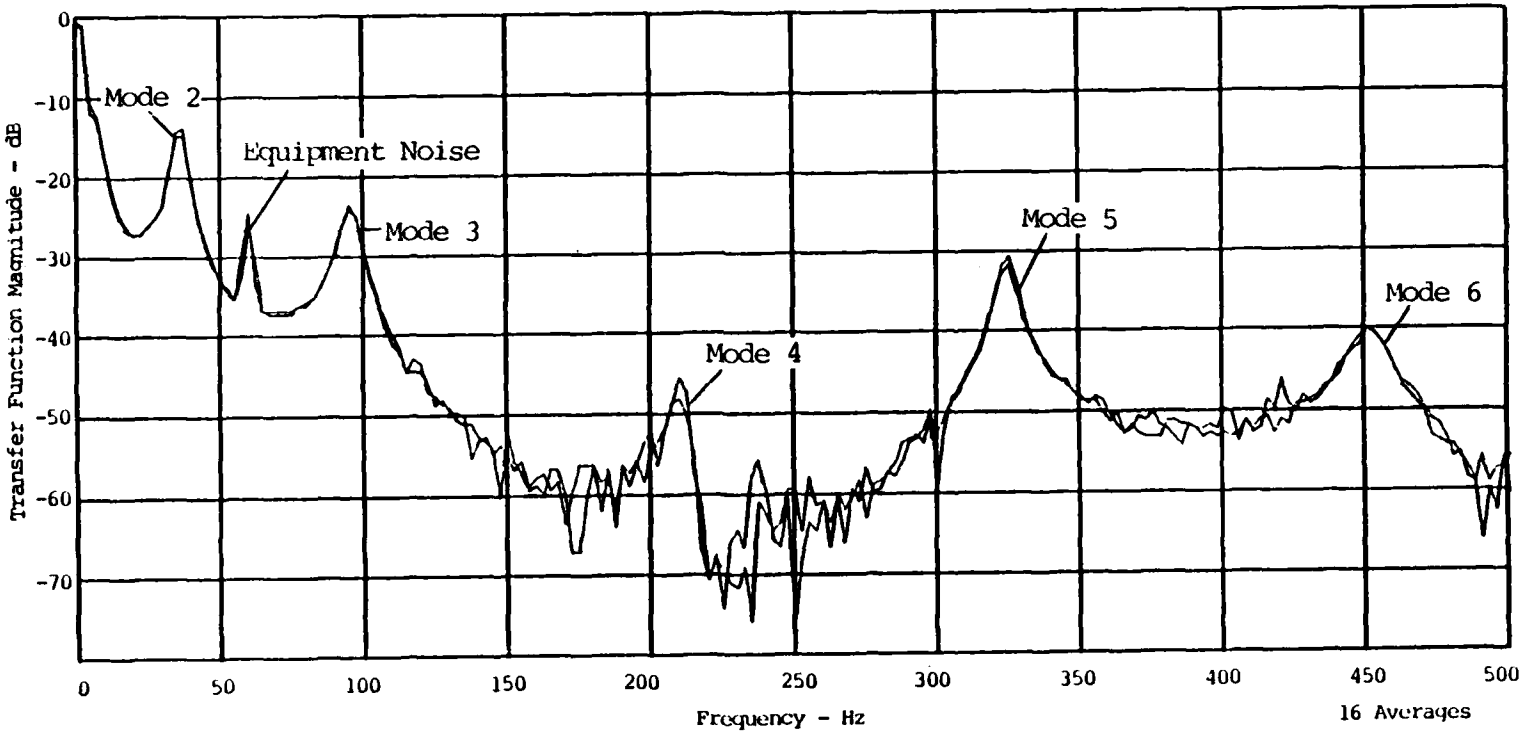

Figure 19. Suppressed Mode Model, R_{uu} = .01, Random Excitation to 500 Hz

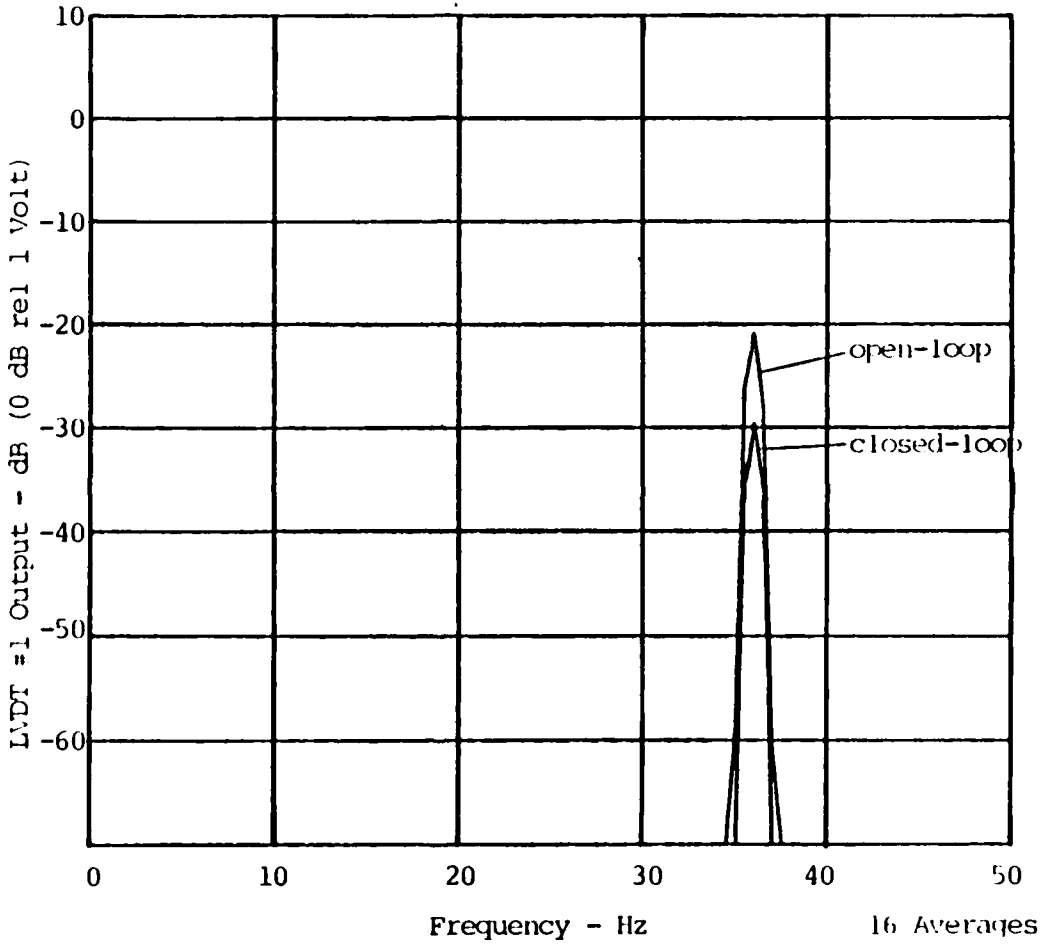

Figure 20. Suppressed Mode Model, R_{uu} = .1, Sine Dwell 36 Hz

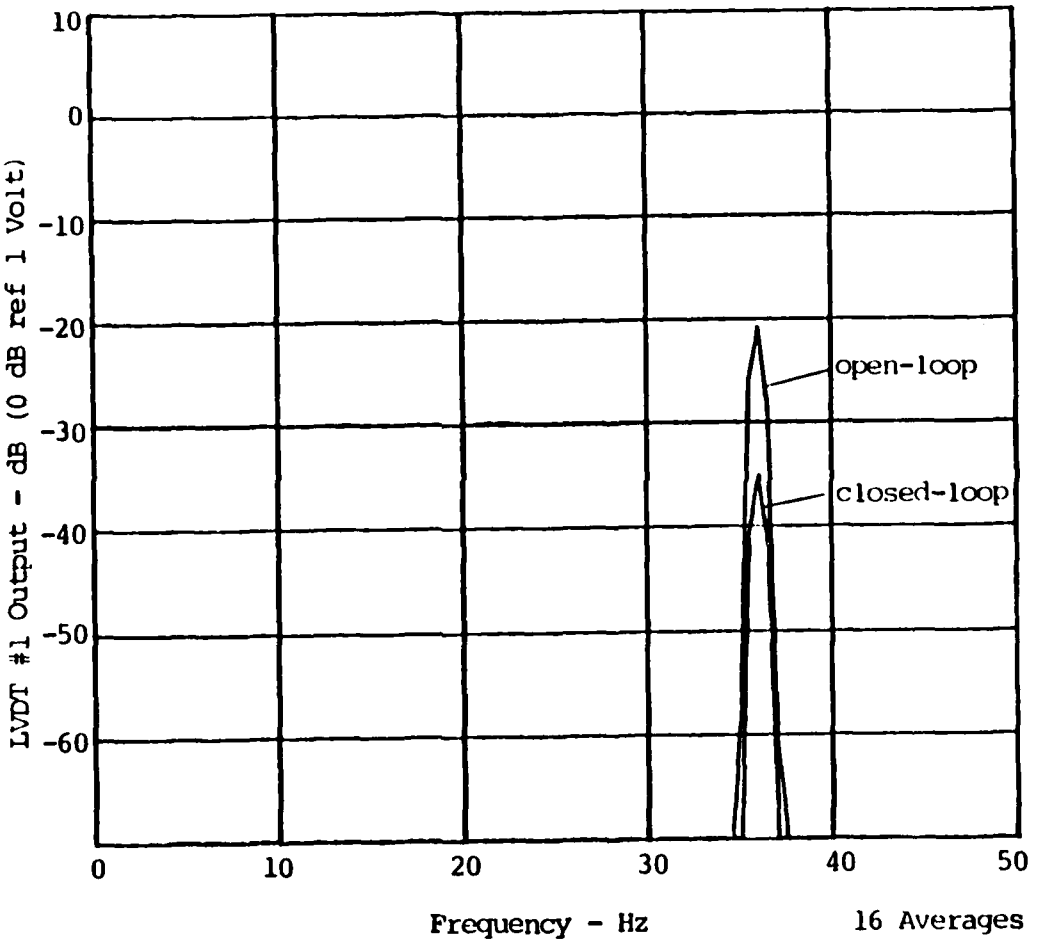

Figure 21. Suppressed Mode Model, R_{uu} = .01, Sine Dwell 36 Hz

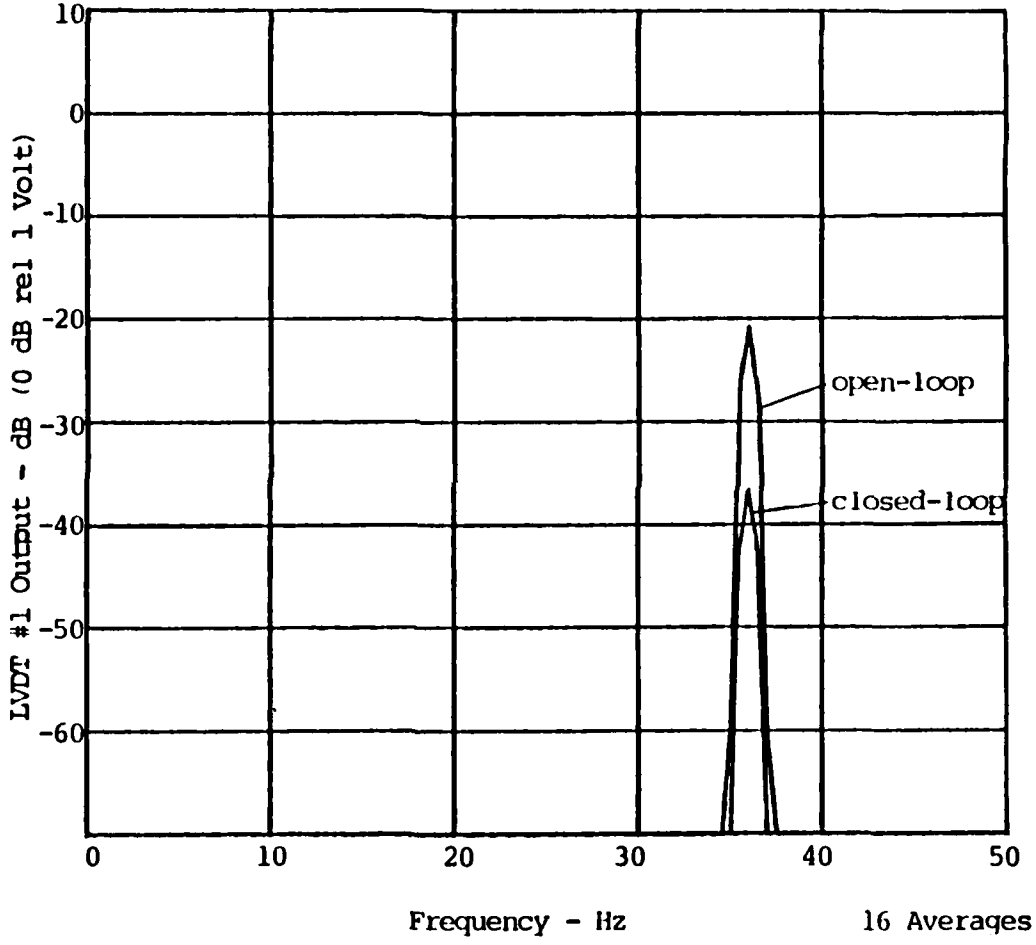

Figure 22. Suppressed Mode Model, R_{uu} = .001, Sine Dwell 36 Hz

are plots of the power output of LVDT #1, not transfer function magnitude plots as from random excitation tests. The excitation force level for the sine dwell results was the same for each of the control designs.

Single Mode Model

Controller models for mode two without suppression were tested in a similar manner. These results are shown in Figures 23 thru 27. Random excitation results are shown in Figures 23 through 25. By increasing the control authority, R_{uu} = .01 to .0001, mode two amplitude was decreased to a greater degree, but mode 1 shows signs of increased frequency and amplitude. See in particular Figure 25 which shows the most dramatic shifts in frequency and amplitude due to higher force levels used in exciting the beam under the same control design shown in Figure 24 (.4 V_{rms} versus .2 V_{rms}). If mode 2 was excited using the random signal generator at .3 V_{rms} or greater, attempts at control for R_{uu} at or below .00005 caused the actuators to overstroke and shut down from excessive first mode amplitudes.

Sine dwell excitation results of the single mode control designs are shown in Figures 26 and 27. Again, successive increases in control authority resulted in decreased displacement in mode two. Decreases of 5 and 8 dB were realized with changes in R_{uu} from .01 to .001 but only small amplitudes in this mode were capable of being excited without driving the system unstable in mode one.

Discussion

The results of this experiment indicate that by eliminating observation spillover from modes 1 and 3, a lower order controller based on mode 2 can work successfully while maintaining a stable system. These results were predicted by computer simulations. Also predicted was the

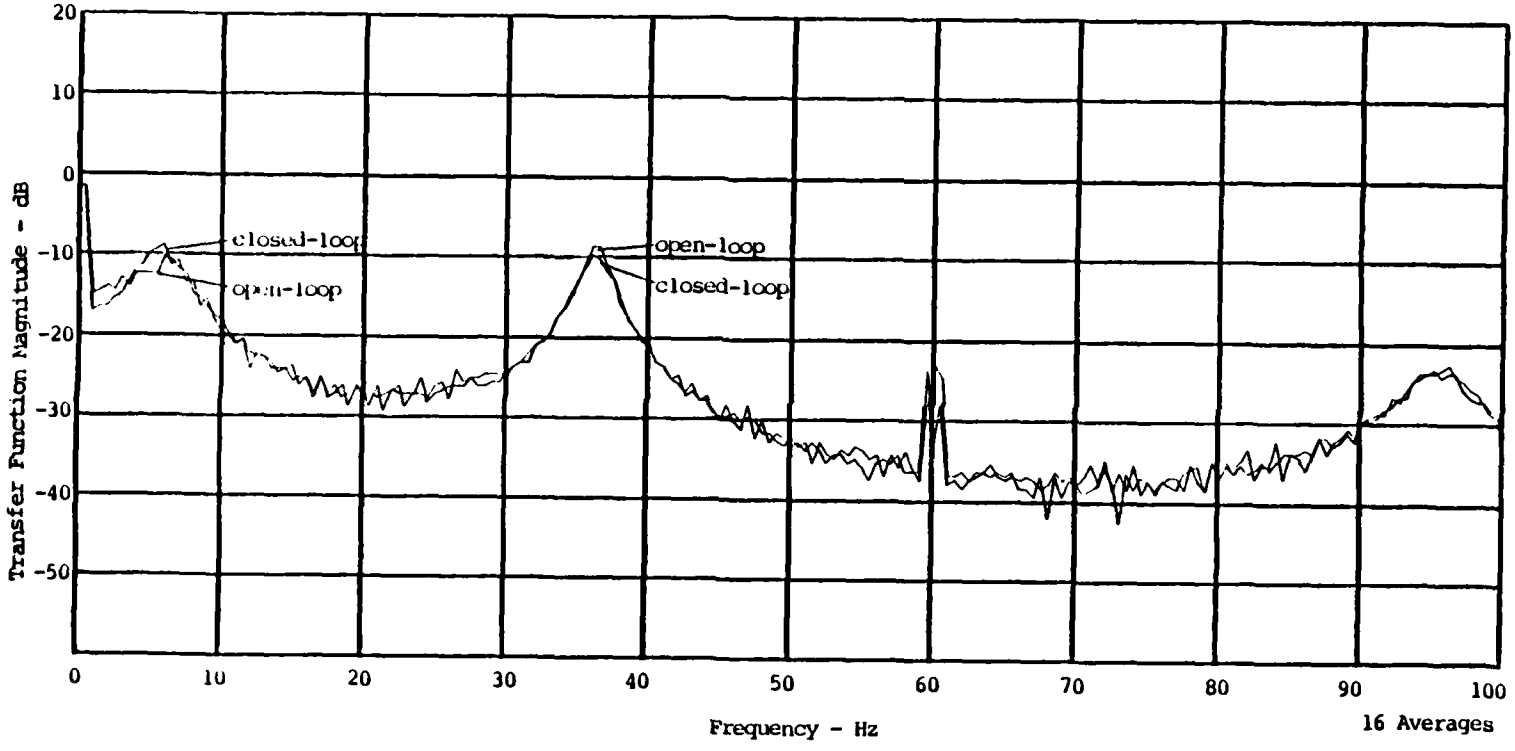

Figure 23. Single Mode Model, Random Excitation, R_{uu} = .1

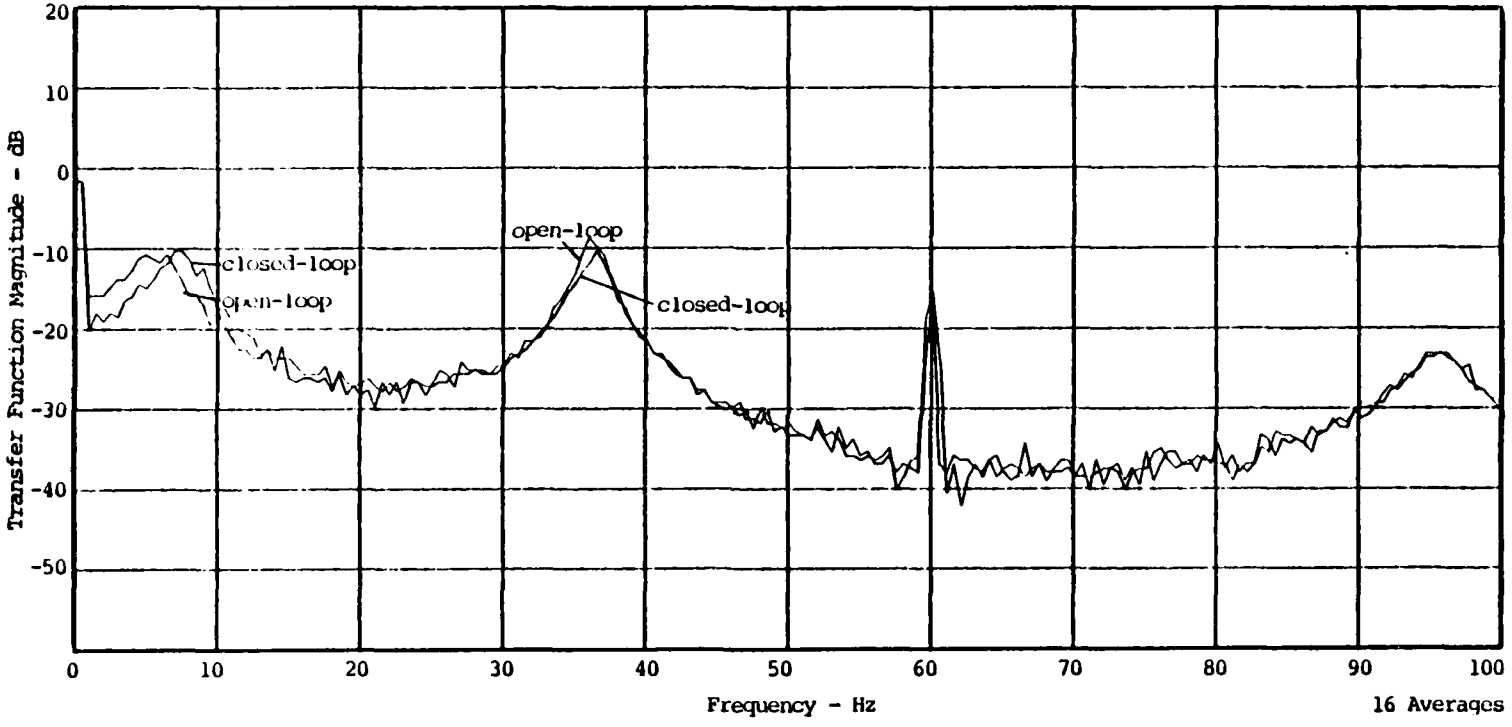

Figure 24. Single Mode Model, Random Excitation .2 V_{rms}, R_{uu} = .0001

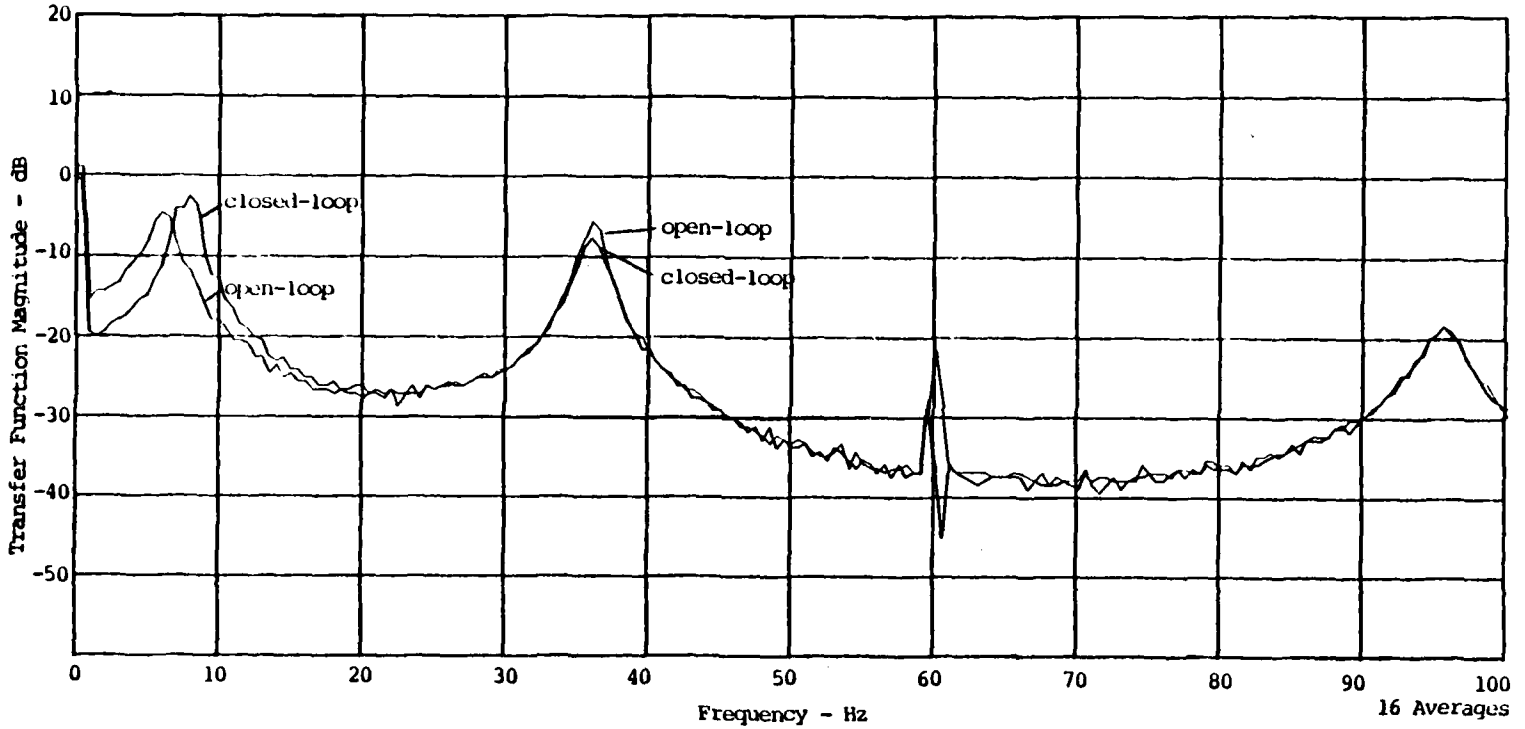

Figure 25. Single Mode Model, Random Excitation .4 V_{rms}, R_{uu} =.0001

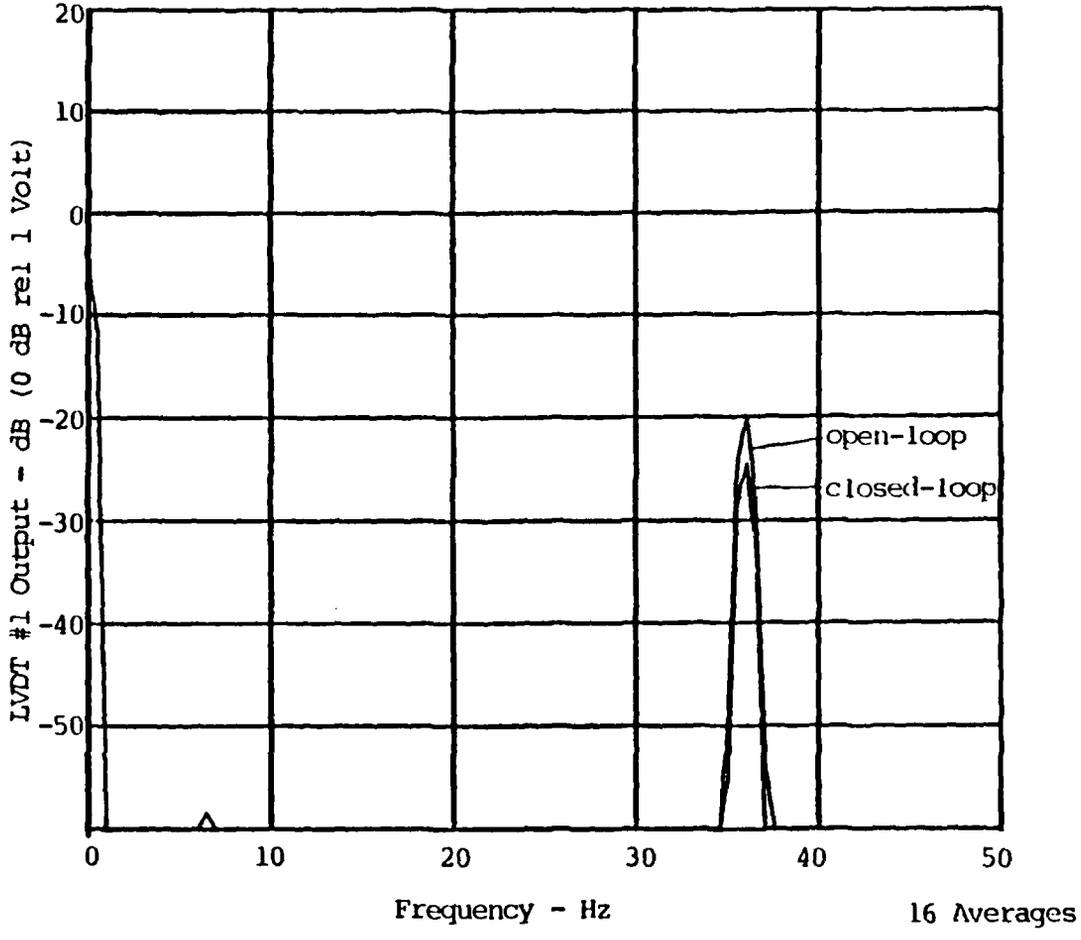

Figure 26. Single Mode Model, Sine Dwell 36 Hz, R_{uu} =.01

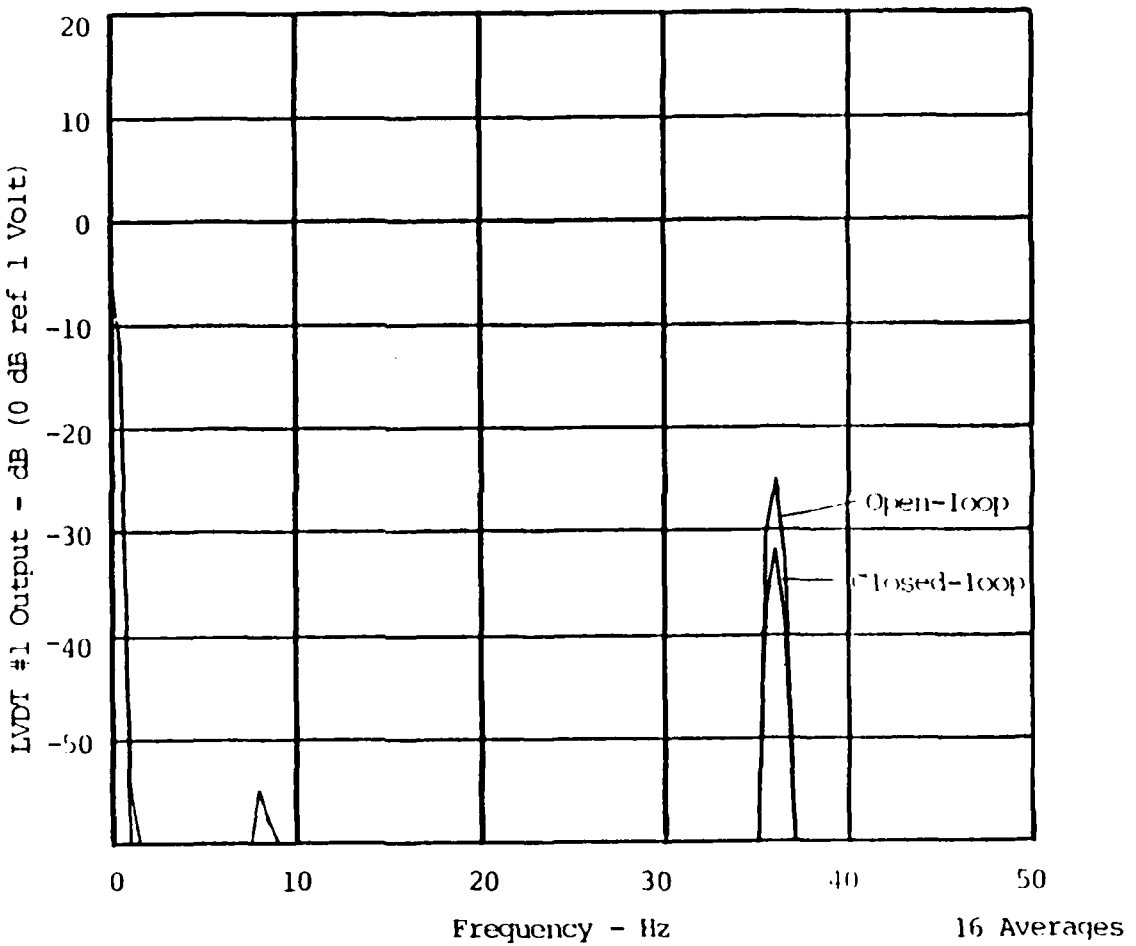

Figure 27. Single Mode Model, Sine Dwell 36 Hz, Ruu = .001

result of a single mode controller, no suppression, decreasing stability in the first mode as control authority was increased.

While the simulations were able to project these trends, exact comparisons between computer generated results and experimentally derived results was not achieved. This was in large part due to the somewhat arbitrary selection of the weighting penalty matricies for Q_{yy} and R_{uu}, and the sensitivity of the actuators.

To try and find the correspondence between simulations and measured results, additional computer simulations were done to determine what R_{uu} factor would give the measured damping results from the suppressed mode model. The specific control vector terms, G, were also calculated for the same purpose. Ratios between the corresponding terms were formed resulting in a range of values over several orders of magnitudes and so no correlation could be drawn. These results are given in Table V.

Table V.
Comparison of Predicted and Measured Results

Experimentally Tested Designs (e)			Computer Predicted Values to Generate the Same Damping (a)		
R_{uu}	G		R_{uu}	G	
.1	.0002	8.14	.165	.0001	1.1439
.01	.0021	1.71	.044	.0005	3.1231
.0001	.208	97.94	.0163	.0013	6.0263

Ratio of Terms

R(e)/R(a)	G(e)/G(a)	
1.65	.5	.14
4.4	.238	1.83
163.0	.006	.06

VIII. Recommendations

The control design used in this experiment was limited to controlling mode 2. New designs could be built to control mode 1, mode 3, or a combination of these modes. Additional experiments in this area could be beneficial, but a different testbed would be recommended.

A new testbed which would permit the experimenter to vary sensor and actuator locations, provide closely spaced modes, and increased number of modes below 100 Hz would provide an ideal environment to thoroughly test the suppression techniques, and possibly decentralized control.

The testbed and equipment should also be well defined such that correlation between simulations and experimentation results are well known. This would dispel any notion that this experiment was fortuitous in that perhaps it just happened to work for the second mode but would not have worked for others.

Bibliography

1 Hungerford, Capt John B. Active Control of Bending Vibration in a Cantilevered Beam, MS Thesis GA/AA/77D-7, School of Engineering, Air Force Institute of Technology (AU), Wright-Patterson AFB OH, December 1977.

2 Coradetti, T., "Orthogonal Subspace Reduction of Optimal Regulator Order, "Proceedings of the AIAA Guidance and Control Conference, Boulder, CO, August, 1979.

3 Balas, M. J., "Active Control of Flexible Systems," Proceedings of the First Symposium on Dynamics and Control of Large Flexible Spacecraft, Blacksburg, VA, pp. 217-236, 1977.

4 Calico, R. A. and A. M. Janiszewski, "Control of Flexible Satellite Via Elimination of Observation Spillover," Proceedings of the Third VPI/AIAA Symposium on Dynamics and Control Of Large Flexible Spacecraft, 1981.

5 Briggs, Maj Hugh C., Experimental Investigation of Large Space Structure Vibration Control, AFWAL-TM-85-251-FIBG, Wright-Patterson AFB OH, Air Force Flight Dynamics Laboratory, December, 1985.

6 Thomson, W. T., Theory of Vibration with Applications, Prentice-Hall, Inc., 1972.

7 Matrix$_x^{TM}$ User's Manual, Integrated System Inc., 1985.

8 Takahashi, Y., Rabins, M., Auslander, D., Control, Addison-Wesley Publishing Co., Reading, MA, 1970.

9 PC-1000 Systolic Array Processor Operations Manual, Systolic Systems Inc., 1550 La Pradera Drive, Campbell, California 95008, Second Edition, 1985.

Appendix: System and Control Design Matrices

This appendix provides the numerical values for the various system matrices, singular value decomposition results, gain matricies, and arrary processor matricies for a suppressed modes model control design. Example printouts from the Compaq computer are also given.

The six mode model was given by

$$A = \left[\begin{array}{cccccc|cccccc} 0 & 0 & 0 & 0 & 0 & 0 & 1 & & & & & \\ 0 & 0 & 0 & 0 & 0 & 0 & & 1 & & 0 & & \\ 0 & 0 & 0 & 0 & 0 & 0 & & & 1 & & & \\ 0 & 0 & 0 & 0 & 0 & 0 & & & & 1 & & \\ 0 & 0 & 0 & 0 & 0 & 0 & & 0 & & & 1 & \\ 0 & 0 & 0 & 0 & 0 & 0 & & & & & & 1 \\ \hline -1463 & & & & & & -.765 & & & & & \\ & -53580 & & 0 & & & & -4.629 & & 0 & & \\ & & -363100 & & & & & & -12.05 & & & \\ & & & -1914000 & & & & & & -27.67 & & \\ & & & & -4649000 & & & & & & -43.12 & \\ & & & & & -9060000 & & 0 & & & & -60.2 \end{array}\right]$$

$$\phi = \begin{bmatrix} .4826 & .2656 & .0809 \\ .5267 & -.1628 & -.2712 \\ .5365 & -.2938 & .3272 \\ .4612 & -.0655 & -.0724 \\ -.5125 & -.1566 & .1505 \\ -.4766 & -.2323 & -.2316 \end{bmatrix}$$

$$[\,m\,] = \text{diagonal}[\,487 \quad 487 \quad 551 \quad 414 \quad 417 \quad 466\,] \times 1E\text{-}05$$

$$B = \left\{\begin{array}{c} 0 \\ 0 \\ 0 \\ 0 \\ 0 \\ 0 \\ \hline 54.538 \\ -33.4292 \\ -53.3212 \\ -15.8116 \\ -37.554 \\ -49.849 \end{array}\right\}$$

$$C = \left[\begin{array}{cccccc|cccccc} .4826 & .5267 & .5365 & .4612 & -.5125 & -.4766 & 0 & 0 & 0 & 0 & 0 & 0 \\ .2656 & -.1628 & -.2938 & -.0655 & -.1566 & -.2323 & 0 & 0 & 0 & 0 & 0 & 0 \\ -.0809 & .2712 & -.3272 & .0724 & -.1505 & .2316 & 0 & 0 & 0 & 0 & 0 & 0 \end{array}\right]$$

Note that the third row elements are the negatives of the associated ϕ terms to compensate for LVDT #3 having an inverted voltage relative to LVDTs #1 and #2.

The suppressed model controller, based on controlling mode two, used the following matricies

$$A_c = \begin{bmatrix} 0 & 1 \\ -53580 & -4.629 \end{bmatrix}$$

$$B_c = \begin{Bmatrix} 0 \\ \hline -33.4492 \end{Bmatrix}$$

$$C_c = \left[\begin{array}{c|c} .5267 & 0 \\ -.1628 & 0 \\ -.2712 & 0 \end{array}\right]$$

and

$$C_s = \left[\begin{array}{cc|cc} .4826 & .5363 & 0 & 0 \\ .2656 & -.2938 & 0 & 0 \\ .0809 & .3272 & 0 & 0 \end{array}\right]$$

The singular value decomposition of the Cs matrix resulted in the following orthogonal matrix of left singular vectors

$$W = \begin{bmatrix} .9071 & -.2484 & .3397 \\ -.1225 & -.9282 & -.3514 \\ -.4026 & -.2772 & .8724 \end{bmatrix}$$

The left singular vector associated with the zero singular values was

$$W_q = \begin{Bmatrix} .3397 \\ -.3514 \\ .8724 \end{Bmatrix}$$

and so the T matrix, where

$$TC_s = 0$$

was

$$T = [\ .3397 \quad -.3514 \quad .8724\ ]$$

The B and C matricies were then multiplied by the sensitivity of the actuators and LVDTs respectively. Based on $Q_{yy} = 10$, the gain matrix K then resulted in

$$K = \begin{bmatrix} .0276 \\ -.1279 \end{bmatrix}$$

For $R_{uu} = .1$, the gain matrix G becomes

$$G = \begin{bmatrix} .0002 & 1.7064 \end{bmatrix}$$

The array processor matrices based on the above design values are then

$$F_{11} = 0$$

$$F_{12} = \begin{bmatrix} .0002 & 1.7064 \end{bmatrix}$$

$$F_{21} = \begin{bmatrix} .0093 & .0096 & .0238 \\ -.2919 & -.3019 & -.7495 \end{bmatrix}$$

$$F_{22} = \begin{bmatrix} .9733 & .001 \\ -52.874 & .9651 \end{bmatrix}$$

Samples of the these matricies as input to the Compaq computer are given on the following pages. Also shown is the data acquisition file which was used. This shows the sampling rate, signal range, and the input and output attenuation gains.

LABPRINT: PC-1000 PRINT UTILITY

FILENAME: b:e21.des

INITIAL CONDITIONS

I	X(I)	Y(I)
1	0.000000E+00	0.000000E+00
2	0.000000E+00	0.000000E+00
3	0.000000E+00	0.000000E+00
4	0.000000E+00	0.000000E+00
5	0.000000E+00	0.000000E+00
6	0.000000E+00	0.000000E+00
7	0.000000E+00	0.000000E+00
8	0.000000E+00	0.000000E+00
9	0.000000E+00	0.000000E+00
10	0.000000E+00	0.000000E+00
11	0.000000E+00	0.000000E+00
12	0.000000E+00	0.000000E+00
13	0.000000E+00	0.000000E+00
14	0.000000E+00	0.000000E+00
15	0.000000E+00	0.000000E+00
16	0.000000E+00	0.000000E+00
17	0.000000E+00	
18	0.000000E+00	
19	0.000000E+00	
20	0.000000E+00	
21	0.000000E+00	
22	0.000000E+00	
23	0.000000E+00	
24	0.000000E+00	
25	0.000000E+00	
26	0.000000E+00	
27	0.000000E+00	
28	0.000000E+00	
29	0.000000E+00	
30	0.000000E+00	
31	0.000000E+00	
32	0.000000E+00	

DESIGN DATA MATRIX

I	J	F(I,J)
3	29	2.079700E-04
3	30	1.706364E+00
29	1	9.300000E-06
30	1	-2.919000E-04
29	3	9.600000E-06
30	3	-3.019000E-04
29	4	2.380000E-05
30	4	-7.495000E-04
29	29	9.733116E-01
30	30	9.650836E-01
30	29	-5.287664E+01
29	30	9.868800E-04
11	29	1.000000E+00
12	30	1.000000E+00

LABPRINT: PC-1000 PRINT UTILITY

FILENAME: b:dac.dac

SAMPLING RATE (Hz)	SIGNAL RANGE (V)
1000	5

CHANNEL	INPUT GAIN	OUTPUT GAIN
1	1	1
2	1	1
3	1	1
4	1	1
5	1	1
6	1	1
7	1	1
8	1	1
9	1	1
10	1	1
11	1	1
12	1	1
13	1	1
14	1	1
15	1	1
16	1	1
17	1	1
18	1	1
19	1	1
20	1	1
21	1	1
22	1	1
23	1	1
24	1	1
25	1	1
26	1	1
27	1	1
28	1	1
29	1	1
30	1	1
31	1	1
32	1	1

Vita

Captain Richard L. Wright Jr. was born 29 April 1956 in Kalamazoo, Michigan. He graduated from high school in Portage, Michigan, in 1974 and attended Michigan State University from which he received the degree of Bachelor of Science in Mechanical Engineering in June 1979. Upeon graduation, he received a commission in the USAF through tht ROTC program. He was assigned to the Flight Dynamics Laboratory of the Air Force Wright Aeronautical Laboratories, Wright Patterson AFB, Ohio, as a systems vibration engineer. He served with the Laboratory until entering the School of Engineering, Air Force Institute of Technology, in May 1984.

Permanent address: 11887 Lakeway Dr.

Plainwell, Michigan 49080

UNCLASSIFIED
SECURITY CLASSIFICATION OF THIS PAGE

REPORT DOCUMENTATION PAGE

1a. REPORT SECURITY CLASSIFICATION: UNCLASSIFIED	1b. RESTRICTIVE MARKINGS
2a. SECURITY CLASSIFICATION AUTHORITY	3. DISTRIBUTION/AVAILABILITY OF REPORT: Approved for public release; distribution unlimited.
2b. DECLASSIFICATION/DOWNGRADING SCHEDULE	
4. PERFORMING ORGANIZATION REPORT NUMBER(S): AFIT/GAE/AA/85D-19	5. MONITORING ORGANIZATION REPORT NUMBER(S)
6a. NAME OF PERFORMING ORGANIZATION: School of Engineering; 6b. OFFICE SYMBOL (If applicable): AFIT/ENG	7a. NAME OF MONITORING ORGANIZATION
6c. ADDRESS (City, State and ZIP Code): Air Force Institute of Technology, Wright-Patterson AFB, Ohio 45433	7b. ADDRESS (City, State and ZIP Code)
8a. NAME OF FUNDING/SPONSORING ORGANIZATION: Flight Dynamics Laboratory; 8b. OFFICE SYMBOL (If applicable): AFWAL/FIBG	9. PROCUREMENT INSTRUMENT IDENTIFICATION NUMBER
8c. ADDRESS (City, State and ZIP Code): AFWAL/FIBG, Wright-Patterson AFB, Ohio 45433	10. SOURCE OF FUNDING NOS. — PROGRAM ELEMENT NO. / PROJECT NO. / TASK NO. / WORK UNIT NO.
11. TITLE (Include Security Classification): See Box 19	
12. PERSONAL AUTHOR(S): Richard L. Wright Jr., B.S., Capt, USAF	
13a. TYPE OF REPORT: MS Thesis; 13b. TIME COVERED: FROM _____ TO _____; 14. DATE OF REPORT (Yr., Mo., Day): 1985 December; 15. PAGE COUNT: 69	
16. SUPPLEMENTARY NOTATION	

17. COSATI CODES			18. SUBJECT TERMS (Continue on reverse if necessary and identify by block number)
FIELD	GROUP	SUB. GR.	Vibration, Controls
20	11		

19. ABSTRACT (Continue on reverse if necessary and identify by block number)

Title: EXPERIMENTAL CONTROL OF SIMULTANEOULSY EXCITED STRUCTURAL MODES

Thesis Chairman: Dr. Robert A. Calico

Approved for public release: IAW AFR 190-17.
9 May 86
LYNN E. WOLAVER
Dean for Research and Professional Development
Air Force Institute of Technology (AFIT)
Wright-Patterson AFB OH 45433

20. DISTRIBUTION/AVAILABILITY OF ABSTRACT	21. ABSTRACT SECURITY CLASSIFICATION
UNCLASSIFIED/UNLIMITED ☐ SAME AS RPT. ☐ DTIC USERS ☐	UNCLASSIFIED

22a. NAME OF RESPONSIBLE INDIVIDUAL	22b. TELEPHONE NUMBER (Include Area Code)	22c. OFFICE SYMBOL
Dr. Robert A. Calico, Prof. of Aerospace Engineering	(513) 255-3069	AFIT/ENY

DD FORM 1473, 83 APR — EDITION OF 1 JAN 73 IS OBSOLETE.

UNCLASSIFIED
SECURITY CLASSIFICATION OF THIS PAGE

This experiment demonstrated the application of a lower order controller. A cantilever beam's second mode was controlled without decreasing stability in the remaining modes. This was made possible by eliminating observation spillover.

Computer simulations were conducted to build control designs and to predict their effectiveness. Modal suppression techniques were used on the first and third modes of a cantilever beam while control was applied to mode two; a three mode model. To measure the effect of the suppression technique, an additional control design based on mode 2 alone was also evaluated.

The simulations indicated that the suppressed modes control design would decrease the second mode amplitude without affecting the first or third modes. Simulations also showed that the single mode model would decrease mode 2 responses but also decrease mode 1 stability. These predictions were verified experimentally on the cantilevered beam.

END

10-86

DTIC